Chapter 3

In vitro identification of inhibitors against *Pf*Pdx1 and their potential MOA

3.1. Introduction

3.1.1. On the inner workings of the PLP synthase complex

The Pdx1 protein combines R5P and G3P, including ammonia provided through the hydrolysis of L-glutamine by Pdx2, to form PLP. Merging of these small molecules occurs in the Pdx1 component of the PLP synthase complex, and how this is coordinated is not entirely understood yet. The Pdx1 reaction mechanism leading to the formation of PLP is fascinating and intricately complex. Some significant findings regarding the inner working of this enzyme are briefly introduced, which alludes to peculiar functions that make it an attractive drug target.

The Pdx1 enzyme perform a multitude of different complex chemical functions including triose- and pentose-phosphosugar isomerizations, condensation of two phosphosugars, imine formation, and closing of the pyridine ring after incorporation of ammonia [119, 162]. The *Pf*Pdx1 protein is highly conserved in organisms utilising the DXP-independent B_6 pathway, including *P. falciparum* parasites [117, 188]. From this high degree of structural conservation it can be deduced that the multiple Pdx1 active sites have an uncompromising nature, and point mutations are not readily tolerated in this gene. This could hold merit in terms of inhibitor design, since fewer incidences of rescue of resistant phenotypes due to point mutations in *Pf*Pdx1 could be expected.

Pdx1 proteins have the ability to utilise alternative substrates such as dihydroxyacetone phosphate (DHAP) and Ru5P as alternative sugars [194]. In particular *Pf*Pdx1 also has this ability [104]. DHAP and G3P are interchangeable triose sugar substrates, and it was shown that Pdx1 contain triosephosphate isomerase (TIM) activity, able to catalyze the conversion of G3P into DHAP [194]. Both R5P and Ru5P are accepted substrates in Pdx1 proteins, however, *B. subtilis* Pdx1 (*Bs*Pdx1) was demonstrated to have a lower K_m value for R5P, which suggests this to be the preferred substrate [195]. Both R5P and Ru5P are incorporated into the final PLP molecule, and the enzyme has been proposed to have R5P isomerase activity.

As mentioned previously, the R5P binding site or P1 site is known from crystallographic evidence [157, 164]. The P2 site or PLP-binding site is located on the surface, and was shown to be solvent accessible with four water molecules complexed with PLP [163]. However, where the R5P and G3P substrates combine, and whether this occurs in the P2 site is not known [163]. A third site or P3 site in which G3P was bound, has been identified, and the G3P molecule had H-bond contacts to E116

and R164 [163]. Equivalent residues of *Pf*Pdx1 that could be involved in G3P binding are R164 and D119.

It is widely accepted that the R5P / Ru5P substrates form imines with an active site lysine as one of the first steps of the reaction mechanism [157, 161, 162]. Hanes *et al.* identified initial reaction ^{13}C-nuclear magnetic resonance (NMR) peaks characteristic of an imine bond between the N atom of lysine and the C1 carbon of the R5P substrate (2 in Figure 3.1) [160]. Additional evidence to support this was shown in the *Pb*Pdx1 structure shown with bound R5P [164]. Earlier structural evidence of Ru5P bound in the *Tm*Pdx1 crystal structure has proven that the molecule is capable of forming an imine with the active site lysine, however substrate isomerisation and reshuffling of Ru5P could lead to reversion into the bound R5P state [157, 160, 194].

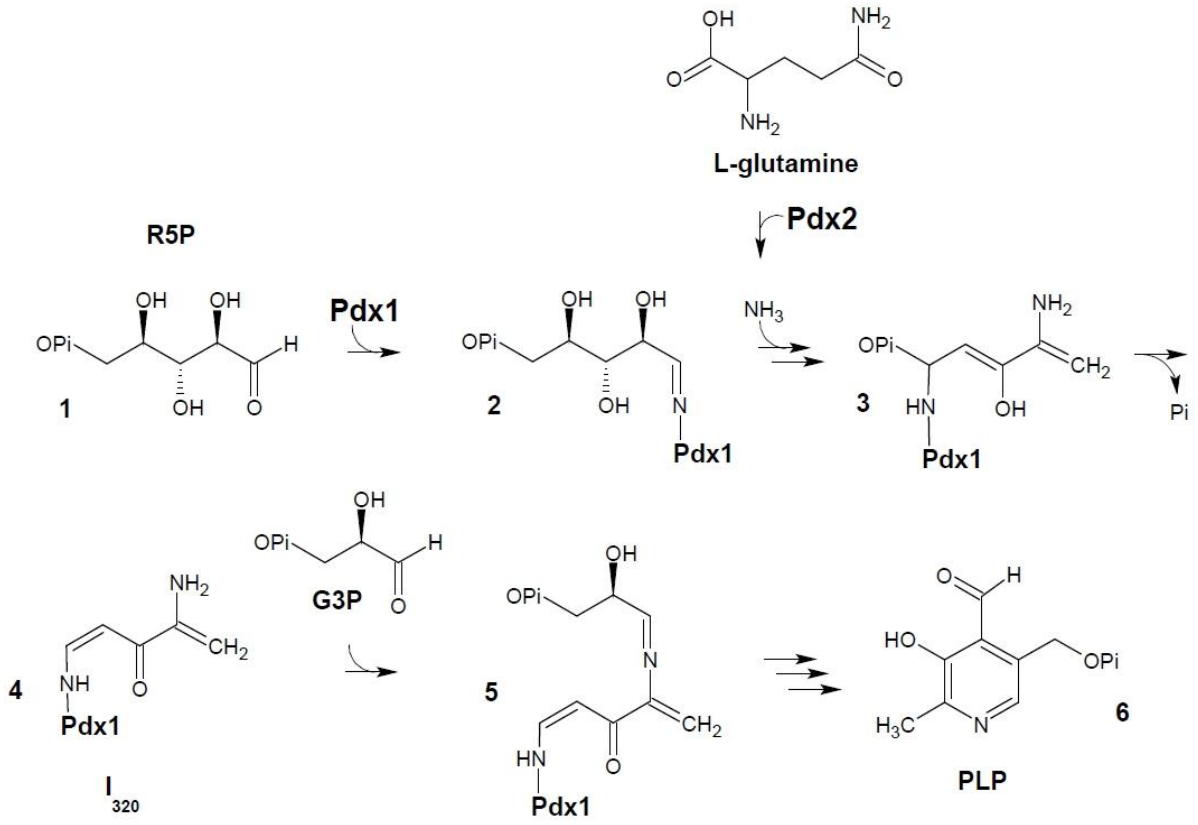

Figure 3.1: The Pdx1 reaction mechanism. Acyclic aldehyde forms of R5P (1) bind via an imine bond to K83 (2). The bound intermediate undergoes isomerization, followed by an additional imine formation with ammonia derived from Pdx2 monomers (3). A C1 to C5 lysine migration also occurs during this step (3). Loss of phosphate results in the formation of I_{320} (4). This bound species has a characteristic absorbance at 320 nm, and forms within the enzyme in the absence of G3P. The I_{320} chromophore undergoes imine formation with G3P (5), and leads to ring closure and formation of PLP (6). This figure was redrawn, as adapted from Hanes *et al.* [160].

Raschle *et al.* identified a novel chromophoric intermediate, called I_{320}, with absorbance maximum (λ_{max}) at 315 nm [162]. This species forms when Pdx1 was incubated with Pdx2 and glutamine with

only the pentose substrate R5P. Formation of the I_{320} chromophoric species was also found to be dependent on the R5P concentration in the presence of the nitrogen source, including ammonium sulphate [162]. Systematically, incubation of R5P with Pdx1 results first in the formation of the imine- or amine-intermediate, then into I_{320} once the ammonium sulphate source was introduced (4 in Figure 3.1) [161, 162]. Hanes *et al.* proved that the I_{320} chromophore was a ketone intermediate species of R5P which further undergoes imine formation with G3P leading to eventual formation of PLP (5 in Figure 3.1) [160, 196]. The I_{320} intermediate can therefore be considered as a marker for R5P binding and an indication that R5P is effectively converted into an intermediate receptive for conjugation of G3P.

Some reshuffling of both the R5P substrate and lysine migration in the R5P-active site has been proposed; Hanes *et al.* showed that there is an imine migration (also called lysine migration) from the C1 of R5P (2 in Figure 3.1) to the C5 (3 in Figure 3.1) after incorporation of ammonia (there are multiple step involved) [160]. This implies that there is a state during the reaction mechanism when an early intermediate form of R5P dissociates from the internal lysine, in order to form the new C5 imine bond with the same lysine. This step could have implications for inhibitor design, and compounds that interfere with imine formation initially as well as during this step could have potential to affect the enzyme activity. A second proposal by Zein *et al.* suggested the possibility of an imine shuffling in *Tm*Pdx1 involving both K81 and K149 residues in *Tm*Pdx1 [157]. The R5P was suggested to be shuffled or transferred to a new site in which the K149 residue forms the imine bond (in this case with the C2 carbon). Mutagenesis of K149 did disrupt PLP formation, consistent with the notion that this residue has direct catalytic involvement [157]. The K149 in *Tm*Pdx1 was suggested to be capable of rotating, coming in close proximity with the Ru5P-K82 imine adduct [157]. Both these proposal suggest that imine formation in the R5P-active site is essential for catalytic conversion of R5P, and compounds that interfere with these steps could be valuable during drug design. Many questions remain regarding the reaction mechanism of Pdx1. The site of G3P-binding in Pdx1 has only recently been proposed and how this substrate is brought into proximity to R5P is not yet known [163]. The active site residues such as D26, K83 as well as K151 are strictly conserved in *Pf*Pdx1 suggesting a similar reaction mechanism.

Recent mutagenesis studies on the *Pf*Pdx1 protein have also highlighted important residues in dodecamer assembly as well as enzyme activity. Two triple mutants of *Pf*Pdx1 were created the DKK (D26A, K83A and K151A) mutant involved mutation of the active site residues, and the RHE (R85A, H88A and E91A) mutant involved residues involved in Pdx1:Pdx1 monomer contacts [133]. Both of these *Pf*Pdx1 mutants were not capable of maintaining dodecameric quaternary structure of the PLP synthase and existed as inactive Pdx1 hexamer and monomer structures,

respectively. [133]. In the DKK mutant the residues that destabilise *Pf*Pdx1 assembly were shown to exclusively the K151A mutation [133]. The monomeric RHE *Pf*Pdx1 mutant, which also did not support Pdx2 activity, suggested that these highly conserved RHE Pdx1:Pdx1 interface residues coordinates Pdx1 assembly to form at least a hexameric Pdx1 crown [133]. The ability of these mutants to form the I_{320} intermediate – a marker of R5P binding - was not tested. The previously created *Pf*Pdx1 DKK and RHE mutants were therefore tested in order to establish the involvement of these residues in the catalytic process of forming PLP.

The C-terminal tail of the *Pf*Pdx1 also contributes to oligomeric assembly and substrate binding. A C-terminally truncated *Pf*Pdx1 (*Pf*Pdx1$\Delta_{273\text{-}301}$ and *Pf*Pdx1$\Delta_{270\text{-}301}$) was monomeric and this 30 amino acid unstructured region is suspected to be involved in initial substrate binding and cooperative assembly of the PLP synthase [182]. This mutant was also unable to form I_{320}, and through long-range interaction is believed to aid in organisation of the R5P active site. Here the *Pf*Pdx1$\Delta_{270\text{-}301}$ mutant was recreated and the catalytic capabilities in terms of PLP and I_{320} formation were confirmed in this study. This also served as a control during analysis of other *Pf*Pdx1 mutants and their ability to form I_{320}. Additionally, the residue located in the P3 G3P binding site was mutated to confirm this residues involvement in PLP formation as well as I_{320} formation. This residue was located more than 20 Å from the R5P binding site, and was not expected to affect I_{320} formation [163]. In the previous chapter, the identification and selection of potential inhibitors of *Pf*Pdx1 were reported. Here the effect of these compounds was tested on purified *Pf*Pdx1 *in vitro*. Some active inhibitors were identified and the potential mode-of-actions of these are discussed further.

3.2. Methods

3.2.1. Expression and purification of *Pf*Pdx1

Plasmids of wild-type *P. falciparum* Pdx1 and Pdx2, as well as K83A, K151A, RHE, ERR, DKK *Pf*Pdx1 mutants, cloned into the pASK-IBA3 vector, were obtained from Knöckel *et al.* [132]. Plasmids were transformed into the *E. coli* BLR (DE3) expression cell line using heat shock transformation. *Pf*Pdx1 plasmid DNA (1 µL or 10 ng) was added to 100 µL heat shock competent cells (prepared as described below), allowing incubation on ice for 30 min. Cells were subjected to a heat shock at 42°C for 60 sec, after which the cells were placed on ice for 2 min. Preheated LB medium (Luria-Berthani sterile medium containing 10% w/v tryptone, 5% w/v yeast extract, 10% w/v NaCl, pH 7.5; 800 µL, 37°C) was added to the transformed cells and the cells grown with shaking (200 rpm) at 37°C for 1 h. Transformed cells (100 uL) were plated out on LB-amp agar plates (LB-broth with 1% w/v agar and 50 µg/mL ampicillin) and grown overnight at 37°C.

For the preparation of heat shock competent cells 5 mL of LB-broth was inoculated with *E. coli* BLR (DE3) and grown overnight at 37°C in a shaking incubator at 200 rpm. The cells were diluted 1:100 into 250 mL fresh LB-broth and were incubated at 37°C with shaking (200 rpm) until an optical density (OD) at 600 nm of 0.5 was reached. The cells were then cooled on ice for 15 min and subsequently centrifuged at 3000*g* for 15 min at 4°C. Whilst working on ice, the remaining pellet was gently re-suspended with 50 mL 80 mM cold $CaCl_2$ and left on ice for 40 min. The cells were centrifuged at 3000*g* for 15 min at 4°C and the pellet was again re-suspended with 5 mL 80 mM cold $CaCl_2$ as well as 2 mL 50% w/v glycerol. Cells were divided into 100 µL aliquots and frozen at -70°C.

Selected single colonies were used to inoculate LB broth (10 mL) containing 50 µg/mL ampicillin (LB-amp) and grown overnight at 37°C. Cultures were diluted 1:100 into LB-amp media and grown to an OD_{600nm} of 0.5. Expression was induced using 200 ng/mL anhydrotetracycline (IBA, Germany) and grown for 4 h at 37°C with shaking. Cells were centrifuged at 2000*g* for 10 min (Avanti J-26 XP, Beckman Coultier) and the remaining pellets were re-suspended using 15 mL buffer W, consisting of 100 mM Tris-HCl, 150 mM NaCl adjusted to pH 8.0 using HCl. Phenylmethylsulphonyl fluoride (PMSF, 0.1 mM) and 5 mg lysozyme (Sigma Aldrich) was added for every 10 mL re-suspended bacterial cell pellet. The re-suspended pellets were sonicated at 40 kHz using pulsing at output 6, duty cycle 40 with 1 min resting intervals on ice (Sonifier 250, Branson). The lysed bacterial mixture was clarified by centrifugation at 50000*g* for 50 min at 4°C (Eppendorf). Strep-Tag fusion proteins were purified using strep-avidin affinity resin according to the manufacturer recommendations (IBA, Germany), as briefly described here. Strep-Tactin®

Sepharose resin (3 mL of 50% suspension) was packed in polypropylene (PP) cartridges containing sintered filters. The resin was equilibrated with 10 column bed volumes (15 mL) of buffer W. The cleared cell lysates (approximately 15 mL) was added to the resin and allowed to elute through at least three consecutive times. Non-specifically adhered proteins were washed off using 3 x 5 mL of buffer W. Elution buffer (2 mL), which consisted of 2.5 mM desthiobiotin and 1 mM ethylenediaminetetraacetate (EDTA) in buffer W at pH 8.0, was eluted through the resin three consecutive times. The resin was regenerated with 15 mL of buffer R, which consisted of 1 mM hydroxy-azophenyl-benzoic acid (HABA), in buffer W at pH 8.0. The columns were finally rinsed with 10 column bed volumes (15 mL) of buffer W.

Protein concentrations were determined using Bradford protein reagent [197], consisting of 0.01% w/v Coomassie Brilliant Blue G-250 (Merck, Germany) dissolved in 4.7 % v/v ethanol (EtOH) containing 8.5% v/v H_3PO_4. Protein containing solutions (10 µL) were diluted with 90 µL buffer W, and pippeted into 1 mL plastic cuvettes (Plastibrand, Brand). Bradford reagent (900 µL) was added and the reactions were incubated at room temperature (RT) for 5 min. Absorbance of the protein-dye solutions were determined at 595 nm and compared to a standard calibration curve of bovine serum albumin (BSA) to calculate the protein concentrations in the analysed samples.

Sodium dodecyl sulphate (SDS) polyacrylamide gel electrophoresis (PAGE) was performed as previously established by Laemmli *et al.* [198], with modifications. Electrophoresis was accomplished in Biometra Minigel protein electrophoresis housings (Biometra, Göttingen, Germany) with plastic gel cassettes of sizes of 8.6 x 7.7 cm (Invitrogen, California, USA). Protein samples were denatured in loading buffer (final concentrations of each component; 50 mM Tris, pH 6.8, 2% w/v SDS, 10% v/v glycerol, 0.02% v/v β-mercaptoethanol, 0.05% w/v bromophenol blue). Samples were boiled for 5 min to denature the proteins. A 10% separating gel was prepared by adding 2.5 mL dH_2O, 1.5 mL of 3 M Tris-HCl pH 8.9, 2 mL acrylamide/bis-acrylamide solution (29.1% w/v acrylamide, 0.9% w/v bis-acrylamide in dH_2O), 60 µL of 10% SDS, 50 µL 10% w/v ammonium persulphate (APS), and a final concentration of 33.5 nM (5µL) *N*,*N*,*N′*,*N′*-Tetramethylethylenediamine (TEMED) to a 50 mL PP tube. This solution was poured into assembled plates, and allowed to polymerise at 4°C for 1 h. The stacking gel component at 5% consisted of 1 mL of 0.5 M Tris-HCl, pH 6.7, 667 µL acrylamide/bis-acrylamide solution, 40 µL 10% w/v SDS, 50 µL 10% w/v APS, and a final concentration of 33.5 nM (5µL) TEMED in a 50 mL PP tube. The solution was cast on top of the separating gel component together with an appropriate comb. Electrophoresis buffer consisted of 25 mM Tris-Cl, 192 mM Glycine, 0.1% w/v SDS. The protein gels were stacked at 80 V, followed by separating conditions at 120 V. The PageRuler unstained protein ladder (Fermentas) with standard reference proteins ranging from 10 –

200 kDa, was used as molecular weight marker. SDS-PAGE gels were stained with Coomassie solution, containing 0.1% w/v Coomassie Brilliant blue R-250 (Serva, Germany), 48% v/v EtOH and 10% v/v glacial acetic acid in dH_2O. Destaining was performed using a solution containing 20% v/v EtOH and 10% v/v glacial acetic acid.

3.2.2. *Pf*Pdx1 activity assays and inhibitor preparation

*Pf*Pdx1 activity was determined spectrophotometrically through detection of a PLP-Tris Schiff base at 414 nm [199]*Pf*Pdx1 activity was assayed in reaction buffer consisting of 100 mM Tris-HCl, 150 mM NaCl at pH 8.0 with purified *Pf*Pdx1 (between 100 – 250 µg, indicated below) including 0.5 mM R5P (Sigma Aldrich, prepared in $dddH_2O$), 0.5 mM G3P (Sigma Aldrich, diluted in $dddH_2O$) and 20 mM NH_4Cl (Merck), unless otherwise stated. Alternatively when the activity of *Pf*Pdx1 was assayed together with *Pf*Pdx2 (between 100 – 250 µg, indicated below), NH_4Cl was replaced with 20 mM L-glutamine (Merck). Blank reactions contained only G3P and NH_4Cl, or G3P and L-glutamine when *Pf*Pdx2 was present. Calibration curves with a PLP standard (Sigma Aldrich, prepared in $dddH_2O$) were made in 100 mM Tris-HCl, 150 mM NaCl pH 8.0, and used to determine the concentration of PLP in the *Pf*Pdx1 incubations. Spectrophotometric measurements at 414 nm, including spectrophotometric wavelength scans and I_{320} measurements, were made using an Uvikon 933B spectrophotometer (Bio-Tek Kontron) in 70µL cuvettes (Plastibrand, Brand). The ability to form PLP was determined by comparing the absorption at 414 nm with a standard calibration curve of PLP in the same buffer conditions. The enzyme activity was expressed in $nmol.min^{-1}.mg^{-1}$.

Both initial inhibitor screening tests as well as inhibitor IC_{50} assays on *Pf*Pdx1 were performed in reaction buffer (100 mM Tris-HCl, 150 mM NaCl at pH 8.0) together with 0.5 mM R5P, 0.5 mM G3P and 20 mM NH_4Cl with 100 µg purified *Pf*Pdx1 in a 250 µL reaction. Assays in which *Pf*Pdx2 was included contained 100 µg of both purified *Pf*Pdx1 and *Pf*Pdx2 in reaction buffer containing 0.5 mM R5P, 0.5 mM G3P and 20 mM L-glutamine. All the inhibitors were prepared in $dddH_2O$, unless otherwise stated. Initial inhibitor screening involved testing inhibitors between 0.5 and 3 mM concentrations. Reactions were set up with the addition of the inhibitor and purified *Pf*Pdx1 or PfPdx1 with *PfP*dx2 occurring last. The enzymes were not pre-incubated with the inhibitors. An uninhibited control reaction was included to ensure active protein was present, and was used as reference to express inhibited reactions as a percentage of the uninhibited control. Inhibitor screening experiments were performed in duplicate on three or more independent occasions.

3.2.3. Mutagenesis of *Pf*Pdx1

Previously created mutants of *Pf*Pdx1 DKK, RHE and ERR were kindly provided by Dr. I.B. Müller and Prof. C. Wrenger [133]. Two additional mutant *Pf*Pdx1 proteins were created in order to study their effects on the enzyme activity and I_{320} species formation. Two different *Pf*Pdx1 mutants were created, the one contained a 31 amino acid deletion on the C-terminal tail (*Pf*Pdx1$\Delta_{270\text{-}301}$) and the other a R164A. Primers designed are listed in Table 3.1. All primers were ordered from Sigma-Aldrich and dissolved in dddH_2O (Millipore) to a final concentration of 300 µM. A working stock solution was prepared by using a 1/10 dilution of the original primer stock solution, with a final concentration of 30 µM.

Table 3.1: **Primers used in mutagenesis polymerase chain reactions (PCR) to create ΔC- and R164A *Pf*Pdx1.** Regions in bold indicate the sites of the introduced modification. The pASK-IBA3 primers were used for automated sequencing.

Primer	Sequence (5' - 3')
ΔC sense	GCGCGCGGTCTCGAATGGAAAATCATAAAGATGATGC
ΔC antisense	GCGCGCGGTCTCAGCG**CTAACATCTAAAAGTATTTTAGGG**
R164 sense	GCTATTAAACATATA**GCA**ACTGTAAATAATGAA
R164 antisense	TTCATTATTTACAGT**TGC**TATATGTTTAATAGC
pASK-IBA3 sense	GAGTTATTTTACCACTCCCT
pASK-IBA3 antisense	CGCAGTAGCGGTAAACG

3.2.3.1. Deletion mutagenesis PCR of *Pf*Pdx1 (*Pf*Pdx1$\Delta_{270\text{-}301}$)

Deletion of the C-terminal tail residues 270 to 301 (*Pf*Pdx1$\Delta_{270\text{-}301}$) of *Pf*Pdx1 was performed using deletion mutagenesis PCR of *Pf*Pdx1 previously cloned in the expression plasmid pASK-IBA3 (IBA, Germany) [132]. The PCR contained 35 ng of expression plasmid with 30 pmol each of the ΔC sense and antisense primer using recombinant *Thermus aquaticus* DNA polymerase in PCR Supermix (Invitrogen). PCR conditions were as follows; 95°C for 3 min, then 35 cycles of 95°C for 30 s, 41°C for 90 s, 60°C for 2 min in a Thermocycler UNO II (Biometra). Parent template was removed from the deletion mutagenesis PCR product using *DpnI* (New England Biolabs). PCR products (20 - 40 µL) were digested with 1 µL of *DpnI* (20 U), whereby reactions were incubated for 2 h at 37°C. Following parent template removal general molecular cloning techniques as described in Section 3.2.4 were followed to ligate the fragments into the pASK-IBA3 expression vector. Fragments were purified according to methodology described in Section 3.2.4.1. The fragments were digested using *BsaI* to enable sticky-end ligation into pre-digested pASK-IBA3 vector as described in Section 3.2.4.3. Digested fragments were again purified, as previously described, and ligated into the vector and transformed into an *E. coli* cloning cell line as outlined in

Section 3.2.4.4. The insertion of the correctly-sized fragments was verified by isolating plasmids and performing RE digestion and automated nucleotide sequencing as described in Section 3.2.4.5

3.2.3.2. Site-directed point mutation of R164 in *Pf*Pdx1

The *Pf*Pdx1 R164A mutant was kindly provided by Dr. I.B. Müller. The mutation was created with R164 sense and antisense primers given in Table 3.1, as described previously [133].

3.2.4. General molecular cloning techniques

3.2.4.1. Purification of PCR and digested fragments

Purification of PCR products was performed using the Pure Link PCR purification kit (Invitrogen) according to manufacturer recommendations, which entailed the addition of 180µL binding buffer to 45 µL PCR samples, and adding the sample to provided spin columns. Columns were spun at 10 000*g* for 1 min, discarding the eluent. Adhered fragments on the columns were washed with 650 µL wash buffer, and centrifuged at 10 000*g* to remove unwanted wash products. The spin columns were additionally spun at 10 000*g* to remove any residual liquids. The PCR products were eluted using 50 µL dddH_2O pre-heated to 50°C.

3.2.4.2. Agarose gel electrophoresis

Gel electrophoresis was performed as previously described by Sambrook *et al.* [200]. A 1% w/v agarose gel was prepared by adding 1 g of agarose (Fermentas) to 100 mL of TE buffer (90 mM Tris, 2 mM EDTA at pH 8.0). The mixture was heated in order to dissolve the agarose, and allowed to cool, after which 5 µL EtBr (10 mg/mL) was added to a final concentration of 0.5 µg/mL. The agarose solution was cast into gel chambers (Biometra, 8.2 cm x 7.1 cm). Samples (5 µL) were mixed with 2 µL sample loading dye (Promega) and loaded into cast gels together with an appropriate DNA molecular weight marker, in this case GeneRuler™ 1000 BP ladder (Fermentas). Electrophoresis was performed for 60 min at 120V in a TE buffer. Bands were visualised under an UV-illuminator to confirm correct PCR products and digested fragments.

3.2.4.3. Restriction enzyme (RE) digestion

The PCR products were digested using *Bsa*I (New England Biolabs, 10 000 U/mL). A typical 100 µL digestion reaction contained 50 µL purified PCR product, 10 µL buffer 3 (New England Biolabs, 100 mM $NaCl_2$, 50 mM Tris-HCl, 10 mM $MgCl_2$, 1mM dithiothreitol (DTT), pH 7.9), 3 µL *BsaI* (30 U) and 1 µL bovine serum albumin (BSA, 10 mg/mL) to a final concentration of 100 µg/mL. Water ($dddH_2O$) was added to a final reaction volume of 100 µL. Reactions were digested at 37°C for 3h. The pASK-IBA3 plasmids were digested to expose sticky-ends prior to ligation with inserts in reactions conditions containing 30 µL vector, 10 µL buffer 3, 3 µL *BsaI* (30 U) and 1 µL BSA with 56 µL $dddH_2O$ digested in conditions similar to above.

3.2.4.4. Ligation

*Pf*Pdx1$\Delta_{270\text{-}301}$ gene constructs were ligated into pASK-IBA3 expression plasmids. Ligation was performed using T4-DNA ligase (New England Biolabs) at 14°C for 24 h in a reaction containing 16 µL purified fragment, 1µL digested pASK-IBA3 plasmid, 2 µL ligation buffer and 1 µL T4-DNA ligase at a 3:1 insert to vector ratio. Plasmids from the ligation reactions were directly transformed into *E. coli* XL10 Gold competent cells (Stratagene) by heat shock transformation using 100 µL competent cells by adding 20 µL of ligation mixture. The cells were incubated on ice then subjected to heat shock as described in section 3.2.1. For plasmid isolation, colonies were selected from the plates and used to inoculate 2 mL LB-amp, and grown overnight at 37°C with shaking.

3.2.4.5. Plasmid isolation

Plasmids were isolated from transformed XL10 gold *E. coli* cells using Gold Plasmid miniprep kit (Peqlab) following manufactures recommendation. Briefly, the 2 mL LB-amp inoculum was pelleted at 10000*g* for 2 min at RT. Solution I (250 µL) was added to the pellets and these were disrupted using vortexing. Solution II (250 µL) was then added and the tubes gently inverted. Solution III (350 µL) was added and the tubes were inverted, after which the tubes were centrifuged at 10000*g* for 10 min. The supernatant was transferred to a PerfectBind DNA spin column and centrifuged at 10000*g* for 1 min, discarding the flow through material. The adhered material on the columns was washed with 500 µL PW plasmid buffer, and centrifuged at 10000*g* for 1 min, discarding the flow-through material. Residual wash buffer was removed by additionally centrifuging the spin columns for 5 min at 10000*g*. Plasmids were eluted from the columns by

adding 50 µL $dddH_2O$, preheated to 50°C, allowing a brief incubation period and then centrifuging the columns at 10000*g* for 3 min.

To verify the correct cloning of the *Pf*Pdx1$\Delta_{270\text{-}301}$ gene construct RE digestion was performed. Purified plasmids were digested using 10 U each of *XbaI* (NEB, 10 000 U/mL) and *HindIII* (NEB 10 000 U/mL), 10 µL of plasmid DNA, together with 2 µg BSA protein (New England Biolabs) and 2 µL Buffer 2 (50 mM NaCl, 10 mM Tris-HCl, 10 mM $MgCl_2$, 1 mM DTT, pH 7.9) filled to a final volume of 20 µL using $dddH_2O$. Fragments were digested at 37°C for 3h. Samples were additionally submitted for automated sequencing (Seqlab, Germany). Reactions were prepared by adding 6 µL of plasmid DNA with 1 µL of IBA3 sense primer, and similarly 1 µL of antisense IBA 3 primer for reverse sequencing reactions. Correct plasmids were transformed into *E. coli* BLR DE3 and purified as described in Section 3.2.1.

3.2.5. Culturing of *P. falciparum* parasites

3.2.5.1. Culture media and culturing conditions

P. falciparum (3D7) parasites were maintained in continuous culture according to Trager *et al.* [201], as modified by Das Gupta *et al.*[201]. The RMPI 1640 culture medium contained 25 mM 4-(2-Hydroxyethyl)piperazine-1-ethanesulfonic acid (HEPES), 10 mM glucose, 20 mM sodium bicarbonate, 25 mM hypoxanthine and 0.5% w/v AlbuMAX II (Invitrogen) at pH 7.4. Parasite cultures were maintained at 2% haematocrit using human O+ erythrocytes in flasks (Nunc) with shaking at 200 rpm at 37°C. The culture media was replaced every second day through centrifugation of the cultures at 3000*g* for 5 min, removing the supernatant, and carefully re-suspending the pellets in the appropriate volume of culture media. Flasks were deoxygenated or gassed using 5% CO_2, 5% O_2 and 90% N_2. The parasitaemia ranged between 1% - 4% depending on the experiments as indicated below.

3.2.5.2. Sorbitol synchronisation

Before IC_{50} assays the synchronicity of the parasite life-stages was controlled by D-sorbitol synchronisation to selectively retain ring-stage parasites, as previously described by Lambros *et al.* [202]. A solution containing 5% w/v D-sorbitol was prepared in PBS and was filter sterilized using 0.22 µM syringe filters (Sartorius). Cultures (50 mL) consisting of mainly ring stage parasites (between 1 to 5% parasitaemia) were centrifuged at 3000*g* for 5 min, after which the supernatants were discarded. The pellets were re-suspended in 5 volumes (10 mL) of the 5% D-sorbitol solution, and incubated at RT for 10 min. The cultures were centrifuged at 3000*g* for 5 min, and the supernatant was removed. The pellets were re-suspended in complete culture media, following gassing procedures as indicated previously.

3.2.5.3. IC_{50} determinations

^{3}H-hypoxanthine incorporation assays were performed as reported by Das Gupta *et al.* [203]. Cultured parasites were washed in RMPI media lacking hypoxanthine prior to IC_{50} determinations. Cultured parasites (250 µL) at initial 2% hemotocrit and 1% parasitaemia were tested in 96 well plate formats with serial dilutions of compound varying from 400 µM – 0.1 µM. After 24 h incubation at 37°C, 100 nCi ^{3}H-hypoxanthine (10 µL of 2.5 µCi/µL) was added. The cells were harvested after another 24 h incubation using an Inotech IH110 cell harvester. The parasite nucleic acid material was collect on pre-wetted (using $dddH_2O$) paper filter mats (Perkin Elmer) using the cell harvester, in which the $dddH_2O$ enables lysing of the cells. The filter mats were subsequently rinsed in $dddH_2O$ and dried under vacuum. The filter mats were dried at 80°C for 15 min then placed in plastic sachets together with 4 mL Ultima Gold™ scintillation fluid (Perkin Elmer) and counted using a Trilux liquid scintillation counter (Wallac). The counts per minute (CPM) generated for untreated parasites within the plates were used as the 100% uninhibited growth control. Assays were performed in triplicate within 96-well plates, and at least three independent biological experiments for each compound.

3.2.5.4. Growth inhibition assays of transfected parasites

Asynchronous parasites, co-transfected with *Pf*Pdx1 and *Pf*Pdx2 contained on pARL1a^{-} vectors with blasticidin and WR99210 antibiotic resistance (kind gift of Carsten Wrenger, Hamburg) together with a Mock cell line containing vector with only antibiotic resistance were maintained in culture, as described previously [141]. The parasite growth was monitored over a period of seven

days (168 h) in the presence of 1 µM 4PEHz, as well as in untreated cultures of the same transgenic cell line. Long term growth assays were performed using 1 mL parasite culture in 12 well format plates (Nunc, Denmark) at 4% haematocrit and a starting 1% parasitaemia. Blasticidin S-hydrochloride (Fluka) and WR99210 were maintained at final concentrations of 2.1 mM (1 µg/µl) and 5 nM, respectively. Both *Pf*Pdx1/*Pf*Pdx2-overexpressing and mock parasites were maintained in culture for 7 days. Spent media was removed daily from suspended erythrocytes by gently tilting the plates, and replaced with fresh media containing both antibiotics. Fresh 4PEHz was added to both treated-*Pf*Pdx1/*Pf*Pdx2 as well as treated-mock parasites every day at a final concentration of 1 µM. The growth rate or parasitaemia was assessed by morphological monitoring and counting of Giemsa (Merck, Giemsa's azur eosin methylene blue solution) stained thin smears using oil immersion light microscopy (Axioskop 20,Zeiss) at 100x magnification, counting ≥1000 total cells (uninfected together with infected) from triplicate slides.

Considering that parasite growth was exponential over time, log transformations were performed to linearize the growth rate data. The growth rate was expressed as the doubling time. The doubling time was a measure of effective doubling of parasite numbers, however considering that the parasite has a 48 hour life cycle and the multiplicity of *P. falciparum* invasions can range from 4 to 16, the term doubling time may be misleading. The doubling time should therefore in this case be interpreted as the effective growth rate of the parasites, and not the actual rate of doubling. Alternatively, the growth rate constant (K), was used to compare the growth of parasites. The effective doubling time has been used to relate different growth patterns in gene disrupted clones of *P. falciparum* by Liu *et al.* [204].

The doubling time or effective growth rate was calculated using the following formula;

$$Doubling\ time = \frac{\ln(2)}{K}$$

In which K represents the growth rate constant with units of h^{-1}. Data (or the cumulative parasitaemia over time) of the 7-day growth inhibition assays were log transformed, and the slope is used to calculate K, by using the following equation;

$$K = \ln(10^{slope})$$

In which slope refers to the slope value from the log graph.

Results were analysed using Graphpad Prism 5, in which the null hypothesis of equal regression lines slopes was tested in a 99% confidence interval ($P = 0.01$). Analysis of covariance (ANCOVA)

was conducted using JMP9 (JMP, Version 9, SAS Institute Inc.), testing whether the slopes significantly differed from each other with $\alpha = 0.05$.

3.3. Results

3.3.1. Expression of *Pf*Pdx1 and initial inhibitor screening

Protein expression and purification of *Pf*Pdx1 and *Pf*Pdx2 was performed as reported previously [158]. The Strep-tag on *Pf*Pdx1 facilitated the purification of the protein on affinity-based resin, and no visible contaminating proteins other than the 37.5 kDa *Pf*Pdx1 were noted on SDS-PAGE with Coomassie staining (Figure 3.2 A). As outlined in Brooks *et al.* during inhibitor screening the linearity of the enzyme assay needs to be to ensure that detection of the product is not compromised or becomes saturated in the product ranges measured [205]. The PLP product is measured as a Schiff-base adduct of Tris at 414 nm [199]. PLP standard calibration curves were linearly correlated with increasing concentrations of PLP, corresponding to the increased formation of a Schiff base between PLP and Tris (Figure 3.2 B). This showed that PLP could accurately be quantified from unknown samples within these ranges.

Ideally during inhibitor screening in the enzyme is maintained in initial velocity conditions, or the linear range where the velocity does not change with time [172]. The relatively low sensitivity for detection of PLP and the relatively slow turnover rate for PLP necessitated using substrate conditions, as well as enzyme concentrations, that led to sufficiently detectable levels of PLP. For this reason initial activity of the enzyme was verified using conditions of 1 mM R5P and G3P with 40 mM NH_4Cl. The formation of PLP by *Pf*Pdx1 was spectrophotometrically monitored as the formation of the PLP-Schiff base at 414 nm over time (Figure 3.2 C). PLP standard calibration curves, such as Figure 3.2 B, were used to calculate the amount of PLP formed by *Pf*Pdx1, and showed that the PLP formed during the reaction fell within the linear ranges for the quantitation of PLP. Linear responses in enzyme activity over time with fixed substrate concentrations showed that no substrate-limiting conditions were reached, and the formation of PLP did not result in product inhibition on *Pf*Pdx1 for the duration of monitoring (Figure 3.2 C). Product inhibition can potentially interfere with interpretation of screening results, and is often associated with plateauing of enzyme activity for extended incubation periods. With linear PLP-formation rates, equating to enzyme activity, this also suggested that the protein remained stable for at least 5 h at 37°C.

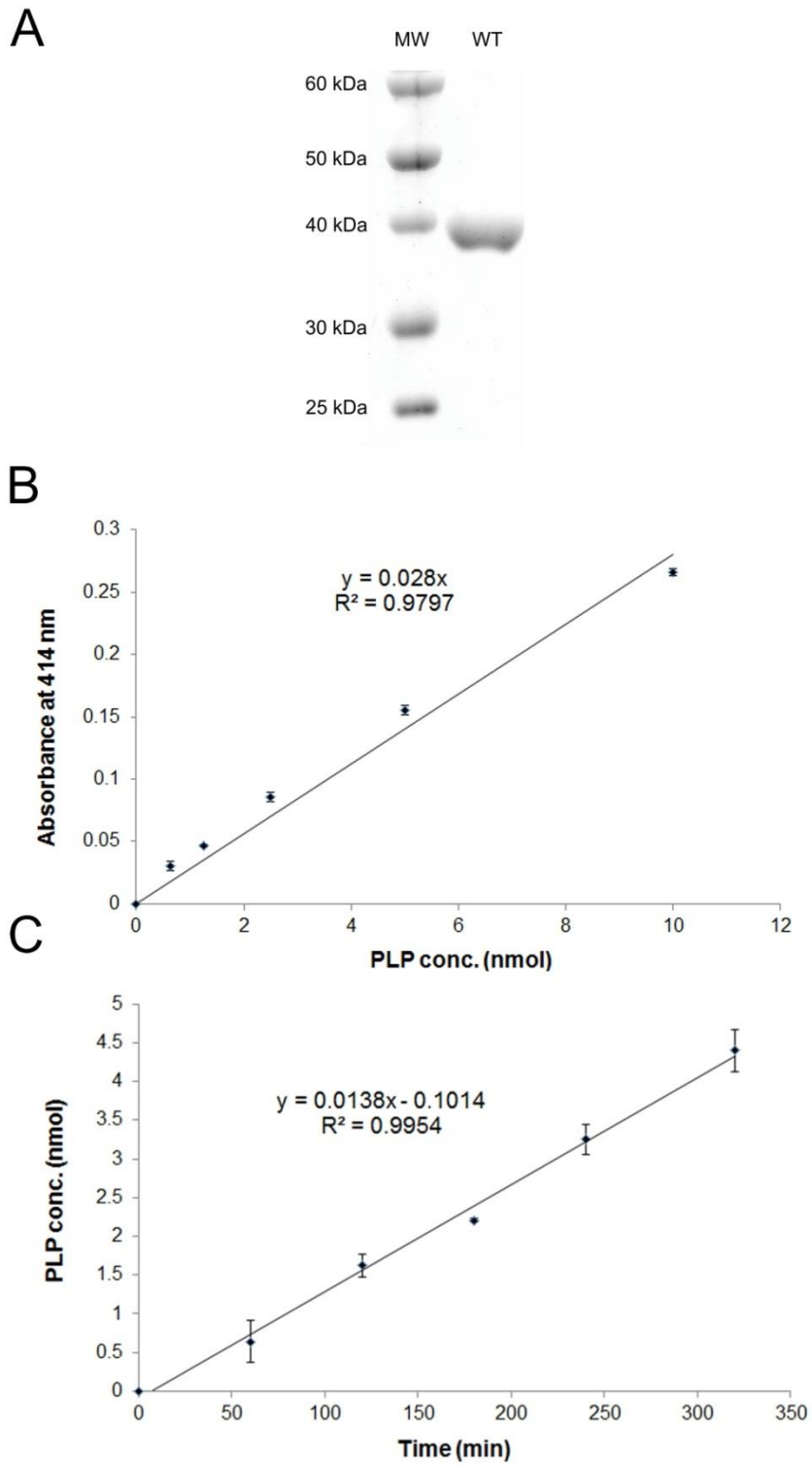

Figure 3.2: SDS-PAGE and enzyme activity of purified *Pf*Pdx1. **A**) Coomassie stained SDS-PAGE gel (black and white image) showing purified protein samples of wildtype (WT) *Pf*Pdx1. One hundred microgram of *Pf*Pdx1 was loaded together with a molecular weight marker (MW). **B)** Standard PLP calibration curve at 414 nm (A_{414}). Error bars indicate the standard deviation from a single experiment derived from triplicate determinations. There was a linear correlation between the PLP concentration and absorbance as reflected by R^2 of the fitted line with 0.97. **C)** *Pf*Pdx1 enzyme activity in reaction buffer (1 mM R5P, 1 mM G3P and 40 mM NH_4Cl) with 100 µg (final concentration 0.125 µg/mL). Aliquots from the incubated solution were removed at hourly intervals. Results represent data from a single experiment with triplicate determinations. Error bars indicate the standard deviation.

The reaction conditions during inhibitor screening were decreased to 0.5 mM R5P and G3P, as well as 20 mM NH_4Cl, with 200 µg of purified *Pf*Pdx1, which still resulted in sufficiently detectable levels of PLP during the reaction incubation times (between 4 – 10 nmol total PLP formed). The reaction times varied between 2 and 3 h at 37°C. The average specific activity of the protein under these conditions was 310 ± 25 $pmol.min^{-1}.mg^{-1}$ protein from more than 10 independently performed experiments. This was marginally lower than previously reported values of 746 ± 76 $pmol.min^{-1}.mg^{-1}$ using 0.5 mM R5P, 1.0 mM G3P and 10 mM NH_4Cl [133, 158], and 695 ± 71 $pmol.min^{-1}.mg^{-1}$ using 1 mM R5P and G3P with 10 mM NH_4Cl [182].

Ligands identified as potential inhibitors of *Pf*Pdx1 by pharmacophore-based drug design (Chapter 2), were tested for their ability to inhibit *Pf*Pdx1. Initial concentrations ranging from 0.5 mM to 3 mM was used for each ligand, in reaction conditions containing 200 µg purified *Pf*Pdx1, 0.5 mM R5P and G3P, as well as 20 mM NH_4Cl. The inhibitors were tested at concentrations equivalent or greater than that of the substrates to promote detection of inhibitory effects on the enzyme. Control reactions excluding inhibitors were included in each screening assay (Table 3.2). Several ligands that were identified contained sulphonate substituent groups (ZINC05273895, TAPS, ACES and ZINC01666581) but did not significantly inhibit the formation of PLP, even when tested at 3 mM (Table 3.2). Additionally, compounds ZINC01586791, ZINC04683167 and ZINC03137815 with carbohydrate backbones also did not show any significant inhibitory action (Table 3.2). NSC163924 with a terminal diol-ester arrangement was the most effective of the conjugated carbohydrates, with a 88% *Pf*Pdx1 activity remaining at 0.5 mM, however this was not statistically significant ($P \geq 0.05$, n = 5). Some compounds containing aromatic rings (ZINC00093092, ZINC04717391, ZINC09680397, ZINC00389974) were predicted to bind within the R5P active site, with the premise that these could potentially mimic PLP in this site. These compounds, however, did not show appreciable inhibitory activity (Table 3.2). The ZINC03897990 compound was coloured with absorption spectra overlapping with that of PLP at 414 nm, and was falsely reflected to increase the *Pf*Pdx1 activity. The pyrimidine compound, ZINC00093092, was shown to significantly (P = 0.046) increase *Pf*Pdx1 activity at 1 mM (Table 3.2).

Table 3.2: Inhibitory activity of *in silico* identified compounds against *Pf*Pdx1. Results are expressed as the average percentage inhibition compared to uninhibited control *Pf*Pdx1 activity calculated from three or more independent experiments performed in duplicate with the standard error of the mean (SEM) indicated. Statistical comparisons, of which the *P*-value is reported, were made using an unpaired two-tailed Student's t-test with $n \geq 3$ in which *P*-values smaller than 0.05 were considered significant.

Compound name or ZINC ID	**Structure**	**Conc. (mM)**	***P*-value**	***Pf*Pdx1 inhibition (% remaining activity)**
ZINC05273895	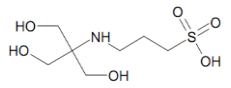	0.5	0.318	96 ± 3
TAPS	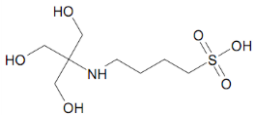	0.5	0.476	103 ± 4
ZINC01666581	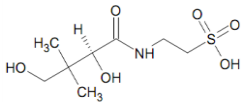	3	0.565	96 ± 5
ACES	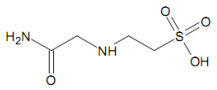	3	0.348	96 ± 3
ZINC01586791	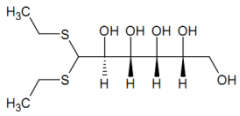	0.5	0.893	99 ± 5
ZINC04683167	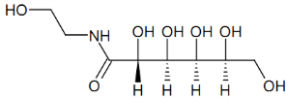	0.5	0.369	107 ± 6
ZINC03137815	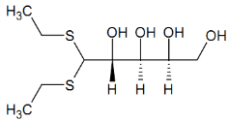	1	0.928	99 ± 7
NSC163924	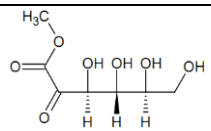	0.5	0.108	88 ± 6
ZINC00093092	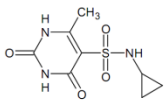	1	0.046	113 ± 2
ZINC03897990	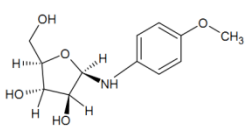	0.5	0.053	200 ± 20 *
ZINC14360284	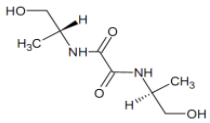	0.5	0.453	110 ± 10

ZINC06269326	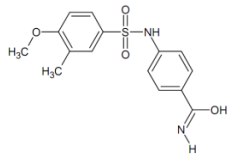	0.5	0.326	107 ± 5
ZINC04717391	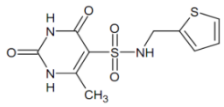	0.5	0.774	99 ± 3
S309737	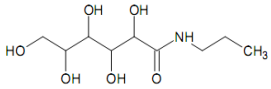	0.5	0.974	99 ± 5
ZINC09680397	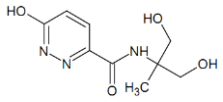	0.5	0.341	95 ± 4
ZINC00389974	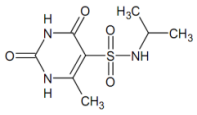	0.5	0.292	105 ± 3

Rationally selected compounds

Compound name	**Structure**	**Conc. (mM)**	***P*-value**	***Pf*Pdx1 inhibition (% remaining activity)**
DR5P	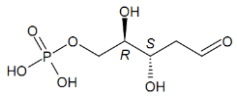	12	0.082	56 ± 4 (Fig 3.6A)
DXP	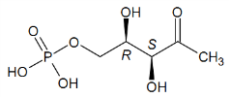	5	0.114	88 ± 4
Fosmidomycin	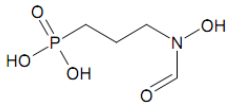	20	0.701 (n = 2)	103 ± 8

*absorbance of compound interfered with detection of PLP.

The overall lack of significant inhibition of *Pf*Pdx1 by *in silico*-identified ligands necessitated additional testing of rationally selected molecules. Analogues of R5P were therefore tested in order to establish the competitive binding interactions since it was anticipated that these analogues could potentially compete or interfere with initial R5P entry into the active site. Compounds tested included 2-deoxy-D-ribose 5 phosphate (DR5P), deoxy-D-xylulose 5-phosphate (DXP), and fosmidomycin (Table 3.2). DR5P showed some inhibitory effect on PLP production (Table 3.2) and was investigated further as discussed below. When tested at 5 mM the acyclic keto-sugar, DXP, marginally decreased *Pf*Pdx1 activity to 88% of that of the uninhibited control *Pf*Pdx1 reactions,

however this was not statistically significant (Table 3.2). The closely related analogue of DXP – fosmidomycin - had no effect on *Pf*Pdx1 activity at 20 mM (Table 3.2).

3.3.2. The inhibition of *Pf*Pdx1 by DR5P, and the effects of related analogues

Spectrophotometric wavelength scans, which allowed the simultaneous monitoring of PLP and I_{320} formation, were used to show that DR5P inhibited *Pf*Pdx1 (Figure 3.3 A). In the presence of DR5P *Pf*Pdx1 showed concomitant decreases in PLP formation as the concentrations of DR5P increased (Figure 3.3 A). The I_{320} formation with DR5P was not significantly altered compared to the uninhibited protein *Pf*Pdx1. The possibility that DR5P could mimic R5P and be incorporated into the final PLP structure prompted further assays with DR5P, as well as other analogues, in which R5P was excluded. However, incubation of *Pf*Pdx1 with DR5P, together with NH_4Cl and G3P did not result in the formation of visible chromophoric species at 414 nm (Figure 3.3 B). DR5P therefore was shown to inhibit *Pf*Pdx1, and could not serve as an alternative substrate in place of R5P. Results suggested that DR5P could mimic R5P and potentially enter the active site, thereby interfering with R5P processing or imine bond formation.

Remarkably the Pdx1 protein is able to isomerise Ru5P to R5P, and also DHAP to G3P. For this reason it was of interest to verify the possibility that other sugar analogues of R5P could serve as a substrate in the *Pf*Pdx1 reaction. The enzyme was incubated with several analogues, including the required G3P and NH_4Cl substrates (Figure 3.3 B and C). In incubations of *Pf*Pdx1 with D-erythrose 4-phosphate (E4P) the formation of a 320 nm chromophoric species similar to incubations with the substrate R5P was noted (Figure 3.3 B). Incubations containing R5P, E4P, DXP or DR5P in the absence of G3P confirmed that only E4P and R5P led to the formation of the chromophore (Figure 3.3 C). These alternative sugars were therefore not considered to support formation of PLP. The effect of E4P on *Pf*Pdx1 I_{320} formation and enzyme activity was investigated further.

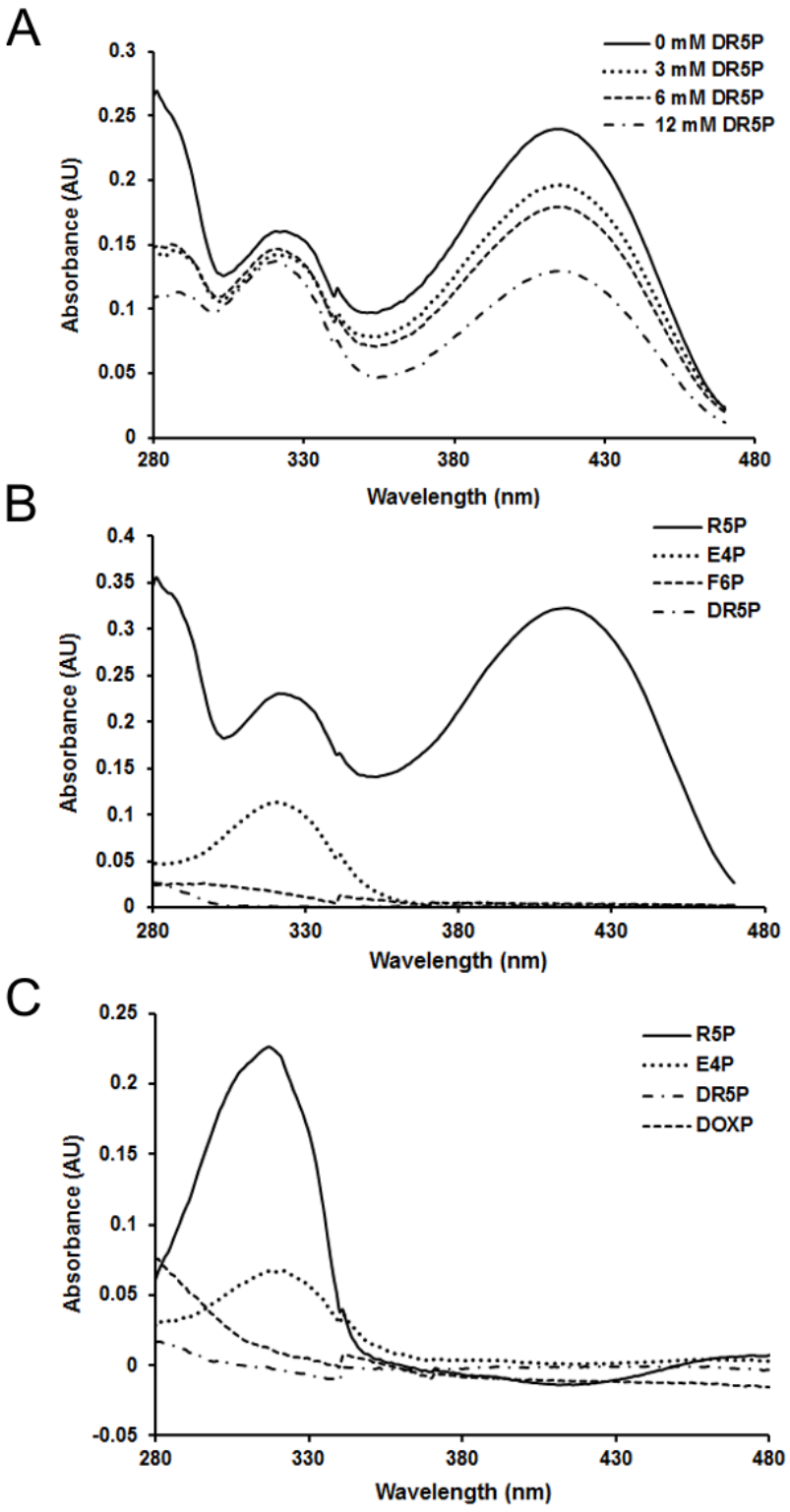

Figure 3.3: Effect of R5P-analogues on *Pf*Pdx1 and I_{320} formation. A) Progressive i**nhibition of *Pf*Pdx1 by increasing concentrations of DR5P in reactions containing 200 µg purified *Pf*Pdx1 with 0.5 mM of each R5P and G3P, using 20 mM NH_4Cl as nitrogen source. Decreased levels of PLP measured at 414 nm correlated with increased concentrations of DR5P.** B) **U**tilisation of alternative sugar **substrates using 200 ug *Pf*Pdx1 incubated with 3 mM R5P, 3 mM E4P, 12 mM D-fructose 6-phosphate (**F6P**) or 12 mM DR5P respectively, in the presence of 1 mM G3P and 20 mM NH_4Cl. Note the 320 nm maximum absorbance only for R5P and E4P.** E4P **was shown to promote formation of an I_{320} species. C) Alternative sugars, E4P (2 mM), DR5P (2 mM) and DXP (2 mM) incubated** with *Pf*Pdx1 in the presence of 0.5 mM G3P and 20 mM NH_4Cl. The positive control included 0.5 mM R5P lacking G3P to

demonstrate formation of the chromophoric intermediate - I_{320}. Solely E4P of the sugar analogues formed the I_{320} species.

3.3.3. Erythrose 4-phosphate inhibits *Pf*Pdx1

E4P was assayed with *Pf*Pdx1 in reaction conditions with R5P, G3P and NH_4Cl to establish whether the compound affected the enzyme activity. Increasing concentrations of E4P was shown to produce the 320 nm chromophoric species (Figure 3.4 A) and also dose-dependently affected PLP production, reflected as decreased 414 nm-absorbance values (Figure 3.4 A). To further elucidate the SAR the dose-response relationship of both E4P and its non-phosphorylated analogue D-erythrose was tested on *Pf*Pdx1 (Figure 3.4 B). The IC_{50} of E4P was calculated as 3.7 ± 0.9 mM and D-erythrose as 160 ± 46 mM (Figure 3.4 B. The calculated IC_{50} of D-erythrose was more than 40-fold weaker against *Pf*Pdx1.

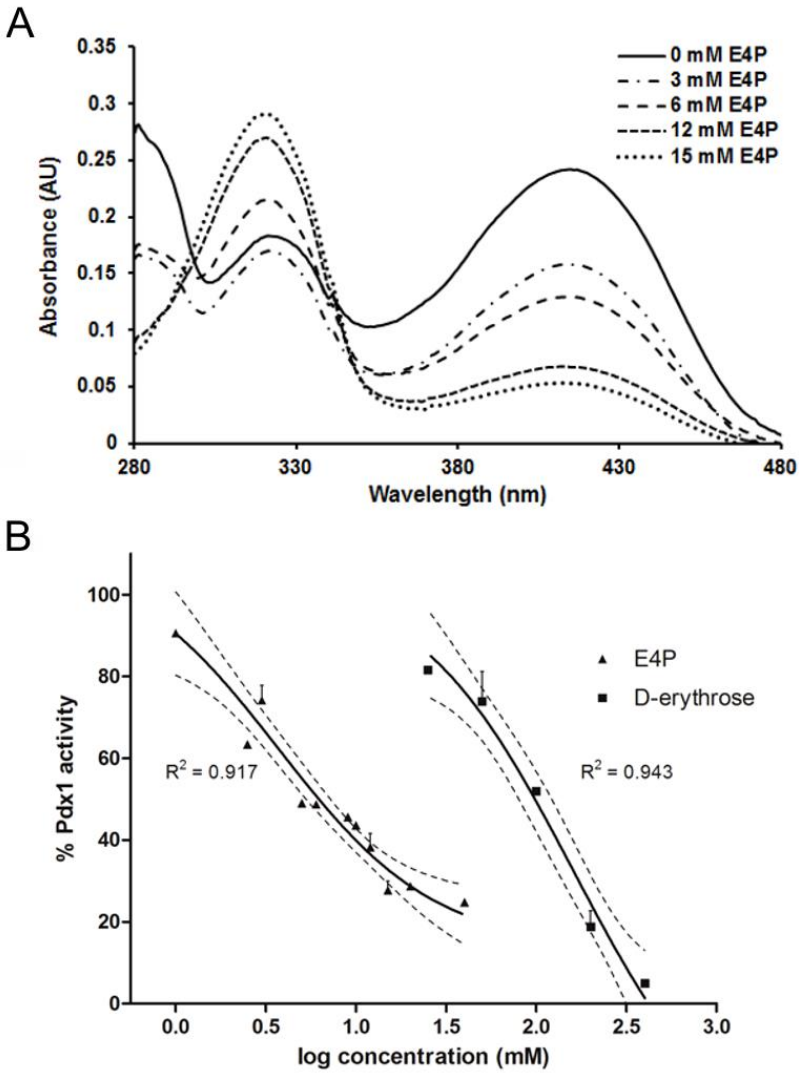

Figure 3.4: Inhibitory effect of E4P on *Pf*Pdx1. A) Representative UV-visible absorbance spectra of *Pf*Pdx1 incubated with increasing concentrations of E4P. Reactions assays contained 0.5 mM R5P, 0.5 mM G3P, 20 mM NH_4Cl with 100 µg of *Pf*Pdx1 and reaction incubation time was 2.5 h at 37°C. **B)** Dose response assays of E4P and D-erythrose on *Pf*Pdx1. Assays contained 100 µg of purified *Pf*Pdx1, with 0.5

mM G3P and R5P, with 20 mM NH_4Cl. Values represent data from three independent experiments performed in duplicate compared to an uninhibited control. Error bars represent the standard error of the mean (SEM) with the 95% confidence interval (CI) presented as dotted lines.

On average at approximately 3 mM E4P (or 375 nmol E4P) there was 50% *Pf*Pdx1 activity remaining compared to the uninhibited control (Figure 3.4 B, with log concentration of 0.477). The total amount of PLP formed in the uninhibited reactions ranged between 9 – 11 nmol (result not shown), and the E4P was therefore present at an excess molar ratio of approximately 37 to 1 compared to PLP. To demonstrate that excess E4P levels did not interfere with the quantitation of PLP incubations with only PLP and E4P in Tris-buffer conditions were set-up (Figure 3.5 A and B). No enzyme was present in these incubations, and served to verify if detection of PLP was affected by E4P.

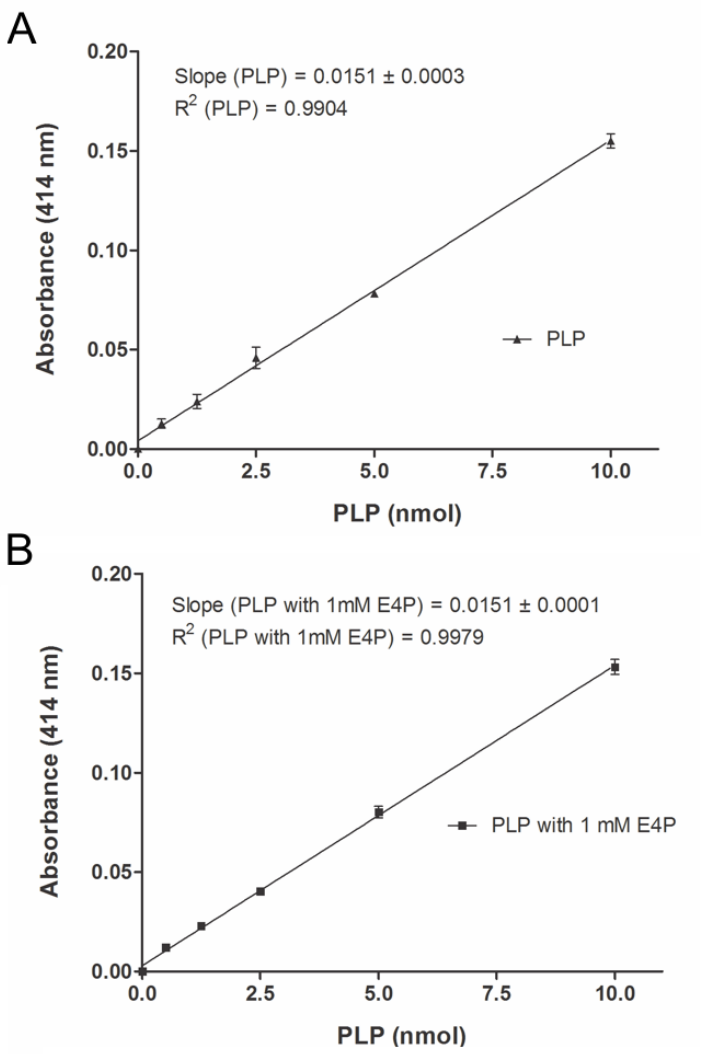

Figure 3.5: Detection of PLP is not affected by E4P. Standard calibration curves of PLP in Tris-Cl buffer conditions with concentrations ranging from 10 µM to 200 µM with **A)** No E4P, and **B)** 1 mM (50 nmol) E4P. Reaction conditions included 0.5 mM R5P, G3P and 20 mM NH_2Cl with incubations at 37 °C for 1.5 h. No *Pf*Pdx1 enzyme was present. Results represent data from four independent experiments performed in triplicate. The E4P-to-PLP molar ratio varied from 80-fold excess to 5-fold excess E4P.

Regression lines of increasing concentrations of PLP, in the absence and presence of molar excess E4P, were generated (Figure 3.5 A and B). Statistical analyses of the linear regression slope and intercepts revealed no significant differences in the slopes of the two different regression lines (P = 0.975). Similarly, ANCOVA showed no significant difference (P = 0.401) between the two regression lines. The lowest point of the PLP standard curve, which has a good fit with the regression line, represented reactions containing 0.5 nmol PLP with 50 nmol E4P, equating to 100-fold molar excess E4P-to-PLP. Even at these high excess E4P conditions the ability to detect PLP was not influenced. If E4P influenced PLP detection the effect would have been noticed as a tapering towards zero at the lower PLP concentration ranges, where conditions of excess E4P are high. This was however not the case. The enzymatic capability of *Pf*Pdx1 to produce PLP was therefore influenced by E4P, leading to further investigations of E4P-analogues and their effect on *Pf*Pdx1, as discussed below.

3.3.4. Characterisation of R5P-I_{320} forming residues

The formation of an I_{320} chromophore, an indication of R5P binding, in *Tm*Pdx1 was previously shown to involve the K83 residue [157]. Similar residues that could be involved in R5P-related I_{320} formation in *Pf*Pdx1 include mechanistically implicated residues such as K83 and D26. Moreover, it was shown that deletion of 31 amino acids from the C-terminal tail of *Pf*Pdx1 abolishes formation of the I_{320} chromophoric intermediate [182], which suggests that I_{320} formation, which follows R5P binding and isomerization, also involves long-range interactions in the protein. Several additional mutant forms of *Pf*Pdx1 were therefore tested to investigate possible involvement of alternative residues in I_{320} formation. These included previously created K83A, K151A, DKK, RHE and ERR *Pf*Pdx1 mutants, as well as the C-terminal tail truncated *Pf*Pdx1$\Delta_{270\text{-}301}$. Additionally, G3P was discovered to occupy a surface exposed site in *S. cerevisiae* Pdx1 (*Sc*Pdx1) [163]. The site for G3P-binding was postulated to include R164, as well as D110 and E116. The equivalent *Pf*Pdx1 residue that could have been involved in G3P-imine formation was R167. To confirm the importance of this residue the enzymatic activity and ability to form the I_{320} specie was tested on a R167A *Pf*Pdx1 mutant (kindly provided by Dr. I.B. Müller).

The *Pf*Pdx1 DKK mutant (D25A, K83A and K151A) did not form the I_{320} species in the presence of R5P, whereas the WT enzyme was catalytically active and in the absence of G3P capable of formatting the I_{320} specie (Figure 3.6 A). Due to the lowered yields from *Pf*Pdx1 DKK expression only 19.8 µg protein could be included in the assays. For this reason lack of I_{320} formation was

confirmed in the K83A and K151A *Pf*Pdx1 mutants, to establish which residue from the DKK mutation plays a role in I_{320} formation. Both the K83A and K151A mutations abolished the formation of I_{320} (Figure 3.6 B). This confirmed the observations in the DKK mutant, and established that both K83 and K151 are essential in initial R5P intermediate formation.

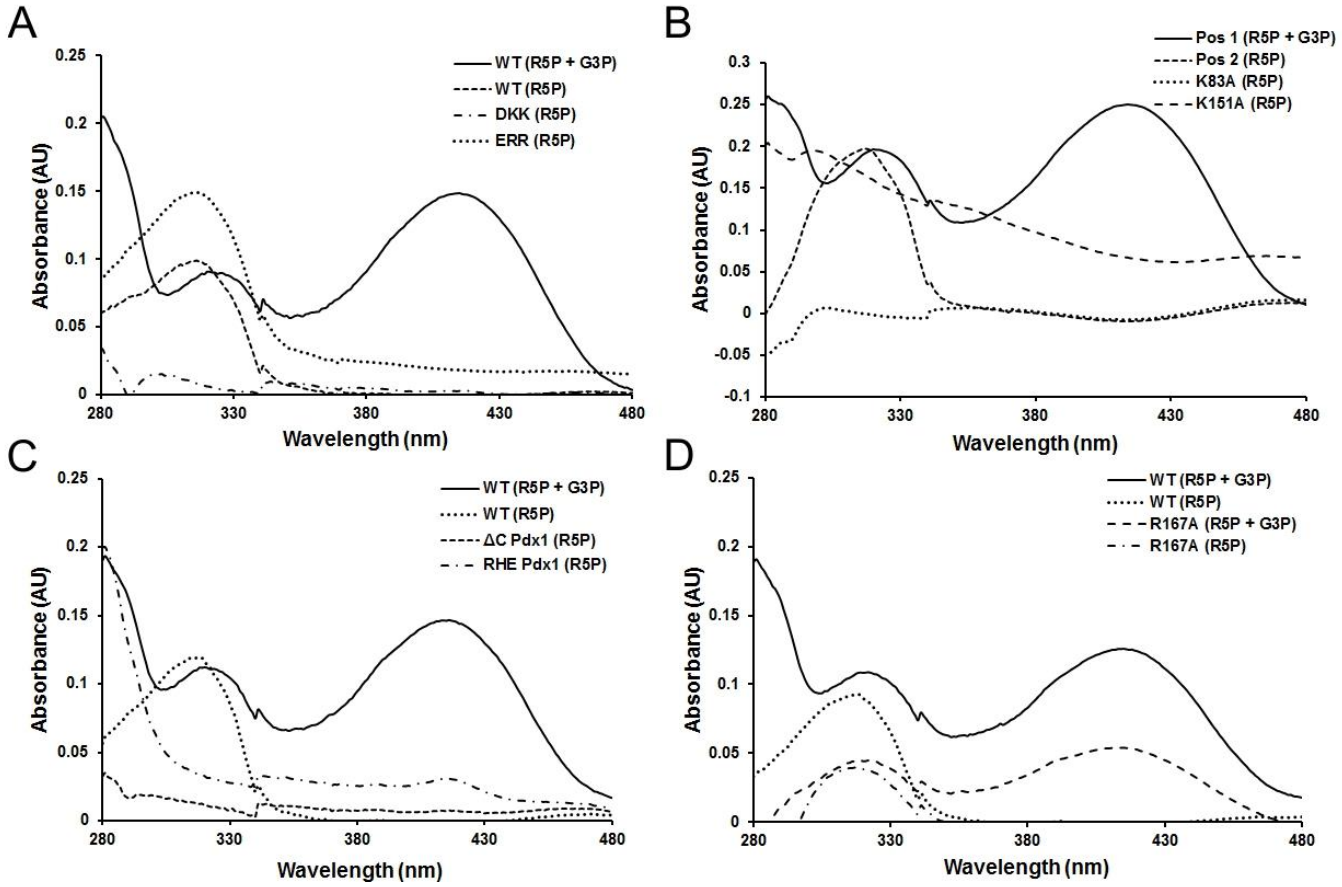

Figure 3.6: Formation of R5P-related I_{320} with *Pf*Pdx1 mutants. A) *Pf*Pdx1 DKK (19.8 µg) and ERR (100 µg) mutants of incubated with 0.5 mM R5P and 20 mM NH_4Cl. Reaction incubation time was 3 h at 37°C. **B)** *Pf*Pdx1 K83A and K151A. The protein mutants (200 µg) were incubated with 0.5 mM R5P and 20 mM NH_4Cl. Higher baseline values for the K151A mutant was attributed to background interferences from the protein purification steps. **C)** *Pf*Pdx1$\Delta_{270\text{-}301}$ and RHE mutants (100 µg each) incubated with 0.5 mM R5P. **D)** *Pf*Pdx1 R167A (100 ug each) incubated with 0.5 mM R5P. In each case positive control reactions included active *Pf*Pdx1 WT (R5P and G3P) with 0.5 mM G3P, 0.5 mM R5P and 20 mM NH_4Cl, as well as *Pf*Pdx1 WT (R5P), in which G3P was omitted to demonstrate active I_{320} formation. Results represent data from experiments performed in duplicate.

The ERR triple mutant *Pf*Pdx1 had comparable I_{320} to WT *Pf*Pdx1, which excluded their involvement in I_{320} formation (Figure 3.6 A). Higher base-line absorbance in the ERR mutant may be attributed to spectral interference which could be related to the properties of the mutant or ineffective removal of some contaminating proteins during protein purification. The relative percentage of the ERR mutant to form I_{320} as listed in Table 3.3 is therefore slightly higher. The truncated C-terminal *Pf*Pdx1$\Delta_{270\text{-}301}$, lacking 31 amino acids, was created, and this was confirmed

through nucleotide sequencing (results not shown) and SDS-PAGE of the recombinantly expressed mutant (Appendix 3, Figure A3.1). The *Pf*Pdx1$\Delta_{270\text{-}301}$ mutant was unable to form the I_{320}, and also not able to generate PLP (Figure 3.6 C). This finding corroborates with previous observations for the C-terminal region of *Pf*Pdx1 [182]. Unexpectedly the RHE *Pf*Pdx1 triple mutant was also unable to form I_{320} or PLP (Figure 3.6 C). Mutation of the R167 residue, believed to be part of the G3P-binding cavity in *Pf*Pdx1, resulted in decreased I_{320} formation (Figure 3.6 D). The R167A mutant was also catalytically impaired, and PLP formation in this variant was around 50% of that of WT *Pf*Pdx1. The properties of *Pf*Pdx1 variants in terms of I_{320} formation, *Pf*Pdx2 activation and PLP formation capabilities are summarised in Table 3.3.

Table 3.3: Relative catalytic capabilities of *Pf*Pdx1 variants. The capability of *Pf*Pdx1 variants to form I_{320} was determined spectrophotometrically and expressed relative to WT *Pf*Pdx1. Additionally, the ability of these mutants to stimulate *Pf*Pdx2 activity and the ability to form PLP is also summarized, with references in brackets. Results represent data from duplicate observations given with the standard deviation.

	R5P I_{320} formation (% compared to WT)	***Pf*Pdx2 activation (% compared to WT)**	**PLP formation (% relative to WT)**
*Pf*Pdx1 WT	100	100 [133]	100
*Pf*Pdx1 ERR	184.3 ± 21.4	104.5 [133]	0 [133]
*Pf*Pdx1 K83A	0.15 ± 0.1	64.6 [133]	0 [133]
*Pf*Pdx1 DKK	24.9 ± 25	103 [133]	0 [133]
*Pf*Pdx1 ΔC	10.1 ± 0.6	99 [182]	0 [182]
*Pf*Pdx1 RHE	28.9 ± 1.6	0 [133]	0 [133]
*Pf*Pdx1 R167A	41.6 ± 6.3	N.D	46.5 ± 3.3

Footnotes: Not determined (N.D.)

3.3.5. E4P analogues and their effect on *Pf*Pdx1

From the E4P lead structure a closely related analogue, 4PEHz [206], was tested on *Pf*Pdx1. The hydrazide derivative was an effective *Pf*Pdx1 inhibitor, and dose-dependently decreased the production of PLP by *Pf*Pdx1 (Figure 3.7 A). This was also accompanied by increases in 320 nm species (Figure 3.7 A). From several independent experiments the IC_{50} of 4PEHz against *Pf*Pdx1 was calculated to be 43 ± 8 µM (Figure 3.7 B). In assay conditions containing both *Pf*Pdx1 and *Pf*Pdx2 with L-glutamine as nitrogen source, the IC_{50} value increased to 16 ± 4 µM (Figure 3.7 C) for 4PEHz. An unphosphorylated analogue of 4PEHz - EHz – was synthesised and used to confirm the importance of the phosphate groups, similar to what was observed for E4P and D-erythrose. The unphosphorylated compound EHz had an IC_{50} of 902 ± 206 µM (Figure 3.7 B) and was more than 20 times weaker than 4PEHz.

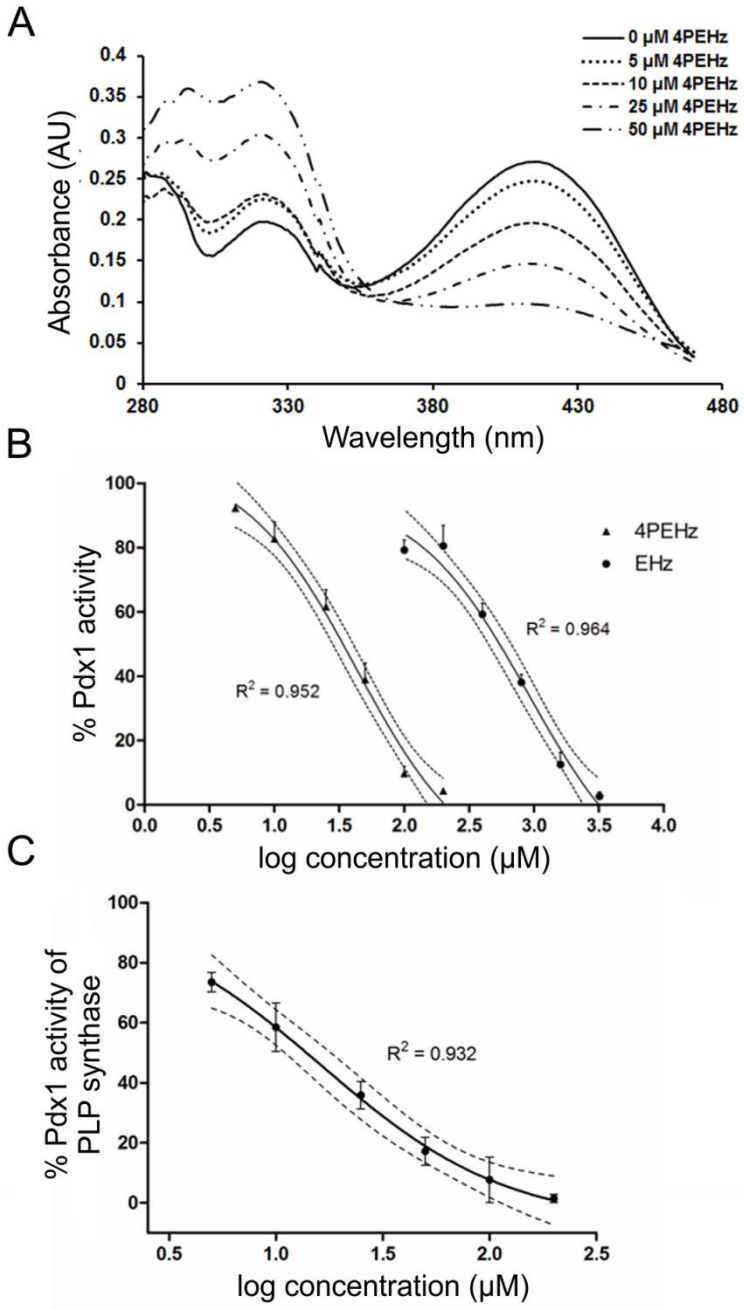

Figure 3.7: E4P analogues and their effect on *Pf*Pdx1. A) Incubation of *Pf*Pdx1 (200 µg) with increasing concentrations of 4PEHz and measured PLP production visible at 414 nm. Results shown represent a single observation from independent triplicate experiments. **B**) Dose-response curves of 4PEHz and EHz inhibition on *Pf*Pdx1 (200 ug). Results were generated from three independently performed experiments, performed in duplicate, with the SEM indicated. The 95% CI is shown as dotted lines. **C)** Effect of 4PEHz on oligomeric *Pf*Pdx1 and *Pf*Pdx2. Reaction conditions included 100 µg of each *Pf*Pdx1 and *Pf*Pdx2 with 0.5 mM R5P, G3P and 20 mM L-glutamine as only nitrogen source. Results were generated from three independent experiments performed in in duplicate, with the SEM indicated. The 95% CI is given in dotted lines.

The inhibitory effect of E4P and analogues against *Pf*Pdx1 are reported in Table 3.4. The trend from the IC_{50} values was that phosphorylated molecules had increased inhibitory capabilities compared to their unphosphorylated counterparts. As mentioned, the unphosphorylated counterparts of E4P and 4PEHz were predicted with lowered binding capability in the *Pf*Pdx1 R5P-binding site (Table 3.4,

see also Chapter 2). This was not so pronounced in the *Pb*Pdx1 model, and rather the unphosphorylated molecules were predicted with overall better LigScores (Table 3.4).

Table 3.4: E4P analogues inhibit *Pf*Pdx1. IC_{50} values were calculated from dose-response curves of the respective compounds incubated with purified *Pf*Pdx1, as reported in the Experimental section. IC_{50} values represent data from three of more independent experiments performed in duplicate, with the SEM indicated. LigScore and Dockscore values were generated from docking in *Pf*Pdx1 (see Chapter 2), with values in parenthesis representing data from docking in *Pb*Pdx1.

Compound	Structure	LigScore1[a]	LigScore2[a]	Dock score[b]	IC_{50} on *Pf*Pdx1
E4P	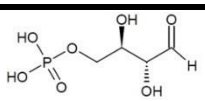	6.40 (3.00)	6.09 (0.41)	85.17 (120.89)	3.7 ± 0.9 mM
D-erythrose	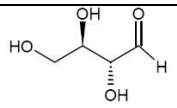	4.74 (3.78)	4.25(2.15)	42.19 (48.20)	160 ± 46 mM
EHz	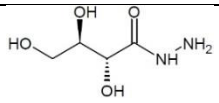	5.34 (4.07)	5.39 (3.46)	53.48 (46.63)	902 ± 206 µM
4PEHz	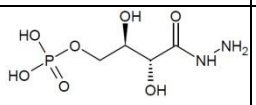	6.55 (3.73)	6.43 (1.46)	98.96 (117.01)	43 ± 8 µM

[a]LigScore1 and LigScore2, with units of pK_i (-log K_i), refers to predicted receptor-ligand binding affinties. [b]Dockscore refers to the unitless rigid body minimisation energy of the final ligand pose calculated during Monte Carlo trials.

3.3.6. 4PEHz and EHz affect parasite growth

Considering the moderate efficacy of 4PEHz and EHz on *Pf*Pdx1, we tested these compounds *in vitro* against *P. falciparum* (3D7) parasites. Parasite growth was monitored as a function of ^{3}H-labelled hypoxanthine incorporation over a 48 h period, after which the cells were harvested and the amount of incorporated material used to describe parasite growth. The 4PEHz compound had appreciable activity against cultured parasites with an IC_{50} of 10.4 ± 1.2 µM, compared to 138 ± 9 µM as determined for EHz (Figure 3.8). Considering that E4P is a natural occurring molecule within the parasites, excess concentrations were not tested on the parasites.

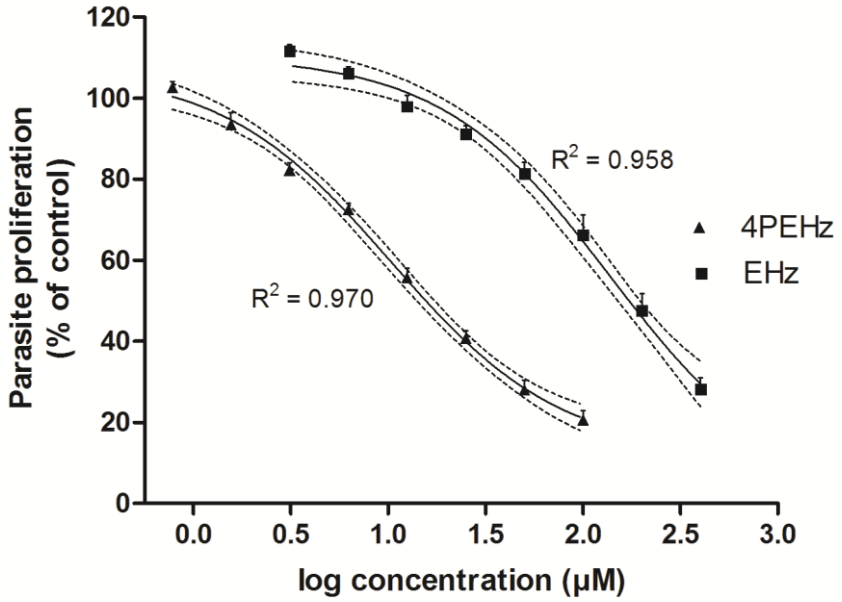

Figure 3.8: Efficacy of 4PEHz and EHz against cultured *P. falciparum* (3D7) parasites. Proliferation was assessed by monitoring the [^{3}H]-hypoxanthine incorporation after 48 h. Values represent data from three of more independent experiments performed in duplicate expressed as the percentage of uninhibited controls.

To further elucidate the effect of 4PEHz *in vitro* and determine the specificity of the compound transgenic *P. falciparum* parasites over-expressing *Pf*Pdx1 and *Pf*Pdx2 (*Pf*Pdx1/*Pf*Pdx2) as well as to control parasites containing a mock plasmid were treated with 4PEHz. The parasite proliferation relative to untreated mock parasites decreased significantly ($P < 0.05$) by 20, 65 and 80% over 48, 72 and 120 h, respectively (Figure 3.9). In contrast, 4PEHz-treated parasites that overexpressed *Pf*Pdx1/*Pf*Pdx2 had unchanged proliferation relative to untreated *Pf*Pdx1/*Pf*Pdx2 parasites (Figure 3.9). This extended period of monitoring was necessary to account for potential delayed drug effects, such as delayed death caused by doxycycline in *P. falciparum* [207], and ensured that the observed rescue effect of *Pf*Pdx1 and *Pf*Pdx2 complementation was sustained through at least three parasite replication cycles. On day 7 the proliferation of the parasites in 4PEHz-treated *Pf*Pdx1/*Pf*Pdx2 parasite appeared to be more diminished compared to untreated cells, however these differences were not statistically significant (Figure 3.9). These results indicate that complementation of PLP metabolism *in vitro* is able to rescue parasites from the effects of 4PEHz which is most likely specifically targeting *Pf*Pdx1 within the parasite.

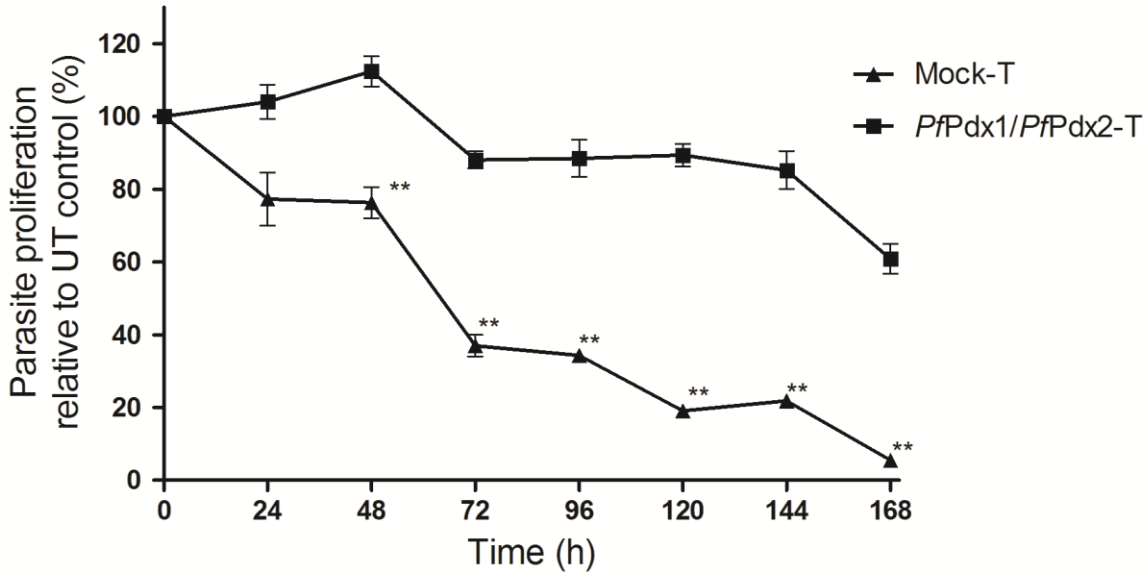

Figure 3.9: Effects of 4PEHz on the proliferation of parasites complemented with *Pf*Pdx1/*Pf*Pdx2- and mock plasmids. The proliferation of mock and *Pf*Pdx1/*Pf*Pdx2 overexpressing parasites treated with 4PEHz are expressed as a percentage relative to the respective UT control cell lines. Results represent averaged values from two independent experiments performed in triplicate with bars indicating SEM and ** indicating $P < 0.05$.

When comparing the slopes of exponential growth curves, and the growth rate constants (K), it was shown that mock-treated parasites (K = 0.0276 h^{-1}) were significantly affected (Figure 3.10 A) compared to untreated mock parasites (K = 0.0412 h^{-1}). The effective doubling time, calculated from the growth rate constant, was 25.10 h in mock-treated parasites compared to untreated parasites with 16.80 h (Figure 3.10 A). Statistical analyses comparing the slopes of the regression lines revealed a significant difference between the slopes (Figure 3.10 A) with $P < 0.0001$. Similarly ANCOVA analyses comparing mock-UT with mock-T revealed that the lines differed significantly (F-ratio probability < 0.0001). These differences in the slope therefore reflected that the growth rates of the mock-treated parasites were significantly diminished compared to untreated parasites. In contrast, the growth rate (K) of the *Pf*Pdx1/*Pf*Pdx2 overexpressing parasites treated with 1 µM 4PEHz (K = 0.0441 h^{-1}) did not differ significantly and remained unchanged compared to that of untreated *Pf*Pdx1/*Pf*Pdx2 overexpressing parasites (K = 0.0457 h^{-1}, Figure 3.10 B). The regression lines of *Pf*Pdx1/*Pf*Pdx2-UT and *Pf*Pdx1/*Pf*Pdx2-T were not significantly different ($P = 0.0138$). Using ANCOVA the regression lines of *Pf*Pdx1/*Pf*Pdx2-T were compared to *Pf*Pdx1/*Pf*Pdx2-UT and did not significantly differ from each other (F-ratio probability = 0.0986). This suggested that complementation of *Pf*Pdx1 and *Pf*Pdx2 rescued the parasites from the inhibitory effects of 4PEHz.

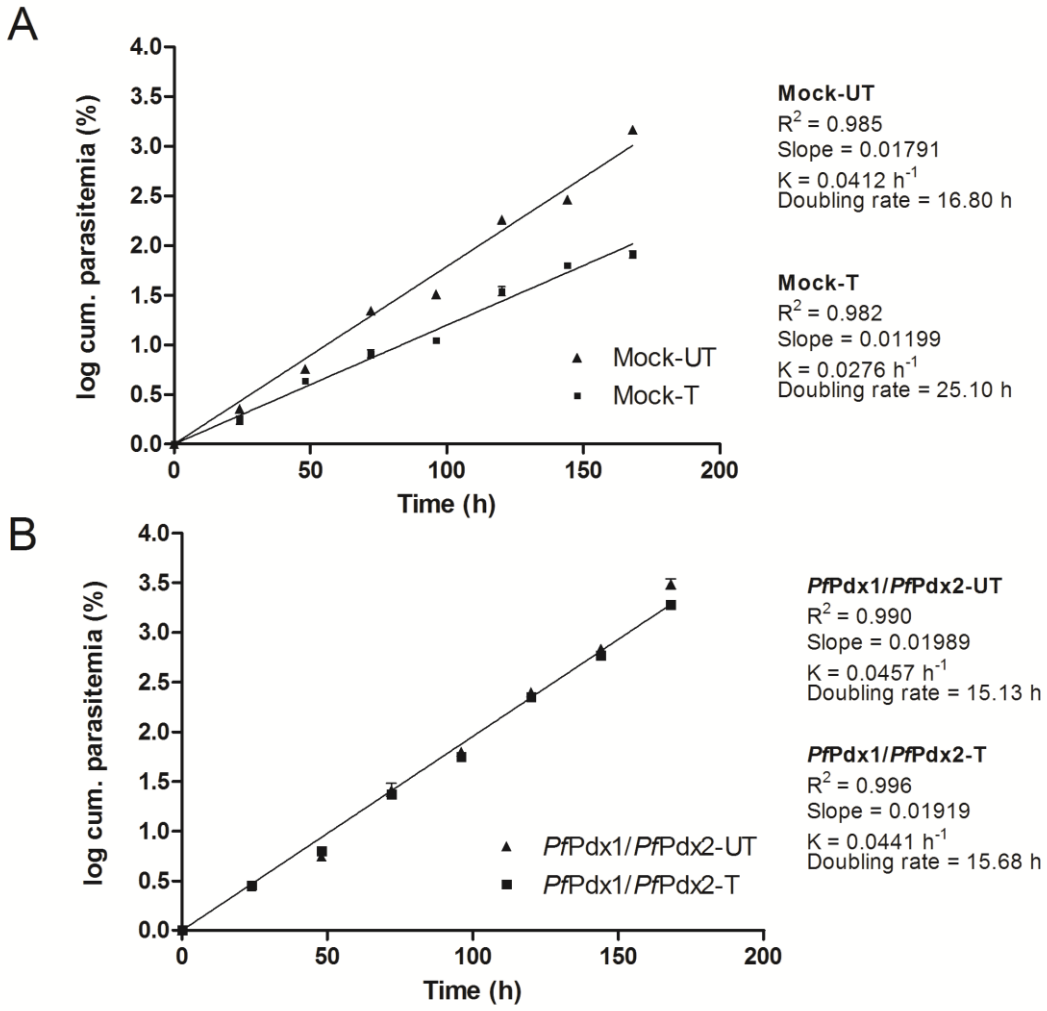

Figure 3.10: Effect of 4PEHz on the exponential growth of transgenic *P. falciparum*. A) Mock control and **B)** *Pf*Pdx1/*Pf*Pdx2 overexpressing cells were treated with 1 µM 4PEHz in continuous culture for seven days as described in Methods section. The cumulative parasitaemia was calculated from the observed parasitaemia by factoring in the dilution during culturing. The data represents average values from two independent experiments performed in triplicate, with the SEM indicated.

The morphological stage composition of the transgenic mock and *Pf*Pdx1/*Pf*Pdx2 parasites were monitored during growth inhibition assays with 4PEHz (Appendix Figure A3.2 and A3.3). The life-stage compositions (percentage of rings, trophozoites and schizonts) of mock-treated parasites was significantly different at 120 h compared to untreated parasites. This was however the only time point affected in the mock-treated parasites. Comparing morphological stages in *Pf*Pdx1/*Pf*Pdx2 parasites, the treatment with 4PEHz did not significantly affect the asexual life-stage compositions (Figure A3.3 A and B).

3.4. Discussion

3.4.1. *Pf*Pdx1 pharmacophore-based ligands

Ligands identified during structure-based pharmacophore screening were tested against purified *Pf*Pdx1. Several sulphonated ligands such as ZINC05273895, ZINC01666581, TAPS and ACES were predicted to bind in the R5P-binding site of *Pf*Pdx1, however did not show appreciable inhibitory activity against *Pf*Pdx1. The hydroxyl substituent in the sulphonate group generally has a pK_a of -1.3, and carries a negative charge at pH 7.0. This group was predicted to mimic the phosphate group of R5P in docking simulations. R5P has two negative charges attributed to the phosphate groups at pH 7.0 and is anchored within the active site with 4 H-bonds to the phosphate group [157]. These molecules, excluding ACES, had bulky terminal groups or tertiary substituted group which could have hindered effective entry into the R5P-active site. ACES contained two amino groups (predicted pK_a of 8.01 and 15.31) which could have influenced the charge of the molecule. At pH 7 the secondary substituted amino group in the aliphatic chain of ACES would be charged, and from inhibition data of *Pf*Pdx1 this is not accommodated in the R5P active site. The other sulphonated compounds, ZINC05273895, ZINC01666581 and TAPS similarly contained secondary amine substituents, and the overall charge of the molecules tended to be neutral or slightly negative. The lack of inhibition by these sulphonated analogues could suggest the charge of the molecule and the stereochemical bulkiness could be important determinants to consider for binding in the R5P site of *Pf*Pdx1.

The polyhydroxyl substituents in R5P, part of the carbohydrate characteristic, functions primarily as H-bond donors, as previously demonstrated in related Pdx1 structures [157]. *Pf*Pdx1 pharmacophore screening successfully identified comparable compounds with polyhydroxyl substituents and docking predicted that some of these could bind in the R5P-active site. These molecules included ZINC0158679, which was the highest scoring compound from pharmacophore screening, as well as ZINC04683167 and ZINC03137815. None of these compounds showed significant inhibitory activity against *Pf*Pdx1 during *in vitro* assays. Binding of R5P (or Ru5P) to K83 requires the formation of a Schiff base, necessitating a terminal aldehyde or ketone arrangement. This could be an important feature in Pdx1 proteins to selectively bind the substrate. The lack of similar groups in the polyhydroxylated analogues could have blocked these from entering the active site.

Several ligands identified from the structure-based pharmacophore screening had aromatic character, such as ZINC03897990, ZINC00093092, ZINC0471739, ZINC09680397 and ZINC00389974. During docking the ZINC03897990 ligand was predicted with better binding

scores compared to R5P. The lack of efficacy of these ligands suggested that these are not effectively accommodated in this site, or any *Pf*Pdx1 site. The pyrimidine compound ZINC00093092 marginally and significantly increased *Pf*Pdx1 activity; the compound could potentially act as an allosteric activator, however no tangible conclusions can be drawn without further investigation.

3.4.2. Substrate preference of *Pf*Pdx1

The Pdx1 reaction mechanism has been elucidated and is summarised in Figure 3.1. A recent mechanistic proposal suggested that initial imine formation with the terminal aldehyde group of R5P occurs with the Pdx1 K83 residues, followed by isomerisation into a Ru5P imine adduct [160]. This bound Ru5P-intermediate is converted into the characteristic I_{320} UV-absorbing chromophore. Hanes *et al.* used isotopically-labelled R5P and NMR to determine the identity of I_{320} [160]. This intermediate forms after the Ru5P-intermediate undergoes a C1 to C5 imine migration, as shown in the second to third transition in Figure 3.1. Loss of the phosphate group from this intermediate results in the formation of I_{320} (Figure 3.1). Only R5P and ammonia are required to form I_{320}, and incubation of Pdx1 with only these substrates produces the characteristic UV-absorbing species.

The fact that Pdx1 has R5P isomerase activity which leads to the formation of I_{320} suggests that the α-hydroxy aldehyde terminal arrangement on R5P, capable of undergoing conjugation, is essential for initial substrate binding and I_{320} formation. [104, 162]. We tested whether other sugar substrates were accepted by *Pf*Pdx1 in the presence of G3P and were expected to be capable of undergoing at least partial imine formation with internal K83 residues in *Pf*Pdx1. DR5P was able to inhibit *Pf*Pdx1 reflecting that some competitive interactions for internal imine formation could exist. The weak inhibition by DR5P could be related to the inability to undergo isomerisation to a Ru5P adduct or the fact that the internal I_{320} specie cannot be displaced by DR5P. With terminal aldehyde functional groups DR5P could compete for K83 Schiff base formation, however, the lack of the C2 hydroxyl substituent could inhibit further isomerisation. This is supported by the fact that DXP, equivalent to the Ru5P scaffold structure apart from the stereochemistry of a single hydroxyl substituent and a terminal ketone group, was not effective at inhibiting *Pf*Pdx1. The initial formation of the Schiff-base requires a reactive aldehyde, which is only present on DR5P, and not DXP. It was therefore surprising that fosmidomycin was ineffective against *Pf*Pdx1, as this compound contains a terminal aldehyde moiety required for initial binding except the one carbon length difference compared to R5P. The molecule however contained more aliphatic character,

potentially prohibiting active site entry, and it was hypothesised that hydrolysable phosphate groups are required for binding as is discussed in more detail later in this section.

E4P was an effective inhibitor of *Pf*Pdx1 with an IC_{50} of 3.7 mM, E4P is structurally similar to both R5P and G3P with a terminal α-hydroxy aldehyde arrangement. The terminal α-hydroxy aldehyde and stereochemical arrangement of the hydroxyl backbone together with hydrolysable phosphate groups in E4P was suggested to be important functional groups to effectively inhibit *Pf*Pdx1. This was supported by the fact that D-erythrose was almost 50-times weaker than E4P emphasising that the hydrolysable phosphate group is also essential.

E4P was also shown to promote the formation of a chromophoric species at 320 nm – this specie formed independently whether *Pf*Pdx1 was present or absent. E4P was previously shown to dimerise into a cyclic hemiacetal form [208]. Moreover, these 320 nm species were formed in the absence of PLP, excluding the possibility of PLP-E4P Schiff-base adducts. Whether E4P dimerises, or reacts with Tris to form these chromophoric species is therefore unknown. In order to demonstrate that the E4P chromophore does not interfere with the detection of PLP molar excess conditions of E4P were used with PLP standard curves. E4P was shown not to interfere with detection of PLP in Tris buffer conditions used during the PfPdx1 enzyme assays. This therefore discounted E4P or Tris-adducts from potentially reacting with PLP, which could have skewed the *Pf*Pdx1 enzyme assays. The results therefore suggested as a linear aldose E4P affected *Pf*Pdx1, possibly by mimicking R5P and could be able to bind to the K83 in the R5P-active site.

Parker *et al.* showed that E4P was capable of forming a Schiff base with a lysine (K186) residue in 3-deoxy-D-arabino-heptulosonate 7-phosphate synthase (DAH7PS) thereby irreversibly inactivating the enzyme [209]. Phosphoglucoisomerases are also inhibited by E4P [210]. The PGI active site are remarkably similar to that of triosephosphate isomerases (TIM), moreover the PGI active site contains lysine residues speculated to be involved in the reaction coordinate [211-213]. Considering the TPI activity of *Pf*Pdx1, capable of utilising both DHAP and G3P, this activity of *Pf*Pdx1 could be targeted by E4P. The definitive location for G3P isomerisation has not yet been established, however this could involve residues located in the P3 site. This therefore allows speculation into the MOA of E4P. There are three potential ways in which E4P can inhibit *Pf*Pdx1; either outcompeting R5P for K83 imine formation, and also undergoing isomerisation. This would affect binding of R5P and lead to disrupted PLP formation. An alternative route could involve E4P binding to the postulated G3P-binding site K120 (equivalent to *Sc*Pdx1 K117) residue, whereby E4P would mimic G3P, interfering with downstream PLP ring-closure steps [163]. The susceptibility of PGI, with TPI

likeness, provides a third alternative, suggesting an unknown site in which isomerisation of G3P occurs, where E4P can potentially bind.

Parasitic E4P is a vital precursor, for the production of chorismate, and downstream phenylalanine, tyrosine and p-aminobenzoic acid utilised for the production of folates [214]. Previous studies have failed to identify homologous sequences of transaldolases in *P. falciparum*, required for the production of E4P from sedoheptulose 7-phosphate [215]. Instead a transketolase (PFF0530w) was cloned and characterised from the parasites and were proposed to produce E4P from F6P and G3P [216]. Earlier studies have reported the presence of 3-deoxy-7-phosphoheptulonate synthase, which condenses E4P and phosphoenol pyruvate as part of the initial stages in the shikimate pathway [217]. Under physiological conditions E4P could therefore regulate PLP production through inhibition of *Pf*Pdx1.

The E4P analogue - 4PEHz - was shown to inhibit *Pf*Pdx1 within low micromolar efficacy. This was also supported by molecular docking simulations. Potentially 4PEHz binds to *Pf*Pdx1 and influences the passage of labile ammonia from the Pdx2 monomer, compared to relatively unrestricted mobility of ammonia in *Pf*Pdx1 only incubations. 4PEHz was previously reported as a weak inhibitor of spinach R5P isomerase with a K_i of 1.8 ± 0.2 mM [206, 218]. Our findings suggest that 4PEHz occupies the same site as E4P, and is supported by the fact that hydrolysable phosphate groups improved binding characteristics. EHz and 4PEHz can potentially form Schiff-bases with PLP through linkage with hydrazide groups. This could be the mechanism by which either compound inhibits the enzyme. These adducts may form in either the P2 and/or P3 sites of the enzyme, leading to PLP-conjugation, and thereby affect the enzyme activity. However, considering that both compounds contain hydrazide functional groups, the difference of inhibitory efficiency suggests some specificity towards *Pf*Pdx1 involving the phosphate group.

During oligomerization of Pdx1 and Pdx2 into the functional PLP synthase Pdx1 activates the glutaminase activity in Pdx2 monomers leading to the formation of a putative opening through which ammonia is channelled [156]. Oligomerization also leads to increased R5P binding affinity in Pdx1 [219]. We noted increased inhibitory efficacy of 4PEHz in the *Pf*Pdx1:*Pf*Pdx2 complex suggesting improved binding interactions of 4PEHz, similar to previous observations for R5P, and further supports that 4PEHz may bind in the R5P binding site.

4PEHz inhibited parasite growth at low micromolar concentrations, compared to the unphosphorylated EHz analogue which was at least 12 fold weaker. The IC_{50} of 4PEHz against cultured parasites was comparable to the IC_{50} against the oligomeric *Pf*Pdx1/*Pf*Pdx2 enzyme complex. Phosphorylated molecules are expected to have poor pharmacokinetic properties, and

passage through the parasite membranes may be hindered. For this reason it was thought that EHz might be a better growth inhibitor than 4PEHz, which was not the case. Some phosphorylated metabolites like AMP can be taken up by parasites, however the exact biological mechanism of transport or protein-mediated transport/uptake still remains unknown [220]. How 4PEHz enters the parasites remains unknown, and ideally isotopic labelling studies would be necessary to study the route of entry.

EHz affected the proliferation of the parasites with an IC_{50} of 138 µM, whereas the IC_{50} for inhibition of *Pf*Pdx1 was 902 µM. The efficacy of EHz *in vitro* was therefore more potent than expected. EHz was predicted to have improved pharmacokinetic properties compared to 4PEHz owed to the lack of the phosphate group, and results presented support the *in vitro* efficacy of EHz. It could however not be ruled out that EHz had alternative intraparasitic targets. 4PEHz was similarly more potent in growth inhibition assays compared to enzyme inhibition results. The potentiated effect of 4PEHz in the parasite could be related to the parasitic dependency on B_6, with inhibition of PLP biosynthesis having severe consequences, resulting in parasite death.

The complementation of PLP biosynthesis through overexpression of *Pf*Pdx1 and *Pf*Pdx2 in *P. falciparum* parasites *in vitro* was previously shown to increase tolerance to cercosporin-induced oxidative stress [140, 141]. Here we similarly observed that parasites which over-express *Pf*Pdx1 and *Pf*Pdx2 were not affected by the *Pf*Pdx1-inhibtor 4PEHz. In contrast, parasites harbouring the same expression plasmid, without *Pf*Pdx1 and *Pf*Pdx2, had reduced growth rates and were significantly attenuated by 4PEHz. The doubling times of the mock parasites were 25.1 h compared to untreated mock parasites with 16.8 h. The doubling times should not be misinterpreted as the time in which the parasite number doubles, rather as a mathematical term which allows comparison of proliferation. The life cycle of the parasite is 48 h, and these parasites cannot double in 16 h. Factored in with the multiplicity of parasite expansion, these doubling times refer to the effective doubling rate over the course of seven days. The overall effect of 4PEHz on the doubling time serves as a comparison between the same cell lines only. 4PEHz therefore affected the doubling times of parasites lacking additional *Pf*Pdx1 and *Pf*Pdx2. Almost 3-fold greater PLP levels were previously reported in *Pf*Pdx1/*Pf*Pdx2 complemented parasites [141]. This complementation of PLP synthesis *in vitro* counteracts the effects of 4PEHz, and suggests that 4PEHz interferes primarily with this part of the parasite metabolism. This suggested that 4PEHz is specific against the *de novo* PLP pathway, and with supporting information from *Pf*Pdx1 inhibitory studies, the compound was suggested to target *Pf*Pdx1 in the parasite. These results support 4PEHz as a novel lead compound for targeting vitamin B_6 biosynthesis within the malaria parasite. How 4PEHz affects functional pathways in the parasite was further analysed using transcriptomics and proteomics in Chapter 4.

3.4.3. Mutagenesis of *Pf*Pdx1

Recent elucidation of Pdx1 has suggested K149 is involved during intermediate transfer towards the P2 site, whereas D26 and K83 constitute the P1 binding site [157, 221]. Our results confirmed residues involved in I_{320} formation include DKK, and more specifically both K151 and K83, equivalent to active site residues *Tm*Pdx1. This corroborates with previous observations elsewhere [157, 162]. Residues located in the PLP-binding site of *Pf*Pdx1 include E136A, R139A and R140A and these were only recently shown to be involved in intermolecular contacts with PLP [157, 163, 221]. The ERR *Pf*Pdx1 triple mutant (E136A, R139A and R140A) was capable of forming the I_{320} intermediate and confirmed the lack of involvement of these residues in R5P isomerisation, however, underscored their catalytic importance more than likely during PLP binding and release.

The mutagenesis of *Pf*Pdx1$\Delta_{270\text{-}301}$ corroborated with previous results which showed that the C-terminal deletion results in abolished I_{320} formation [182]. Additionally, the R164 residue which is proposed to be part of the G3P binding site or P3 site in Pdx1 was also suggested to be important in I_{320} as well as PLP formation. This residue is part of the Pdx1:Pdx1 contact region which G3P is located, and in the *Sc*Pdx1 structure this residue is located more than 20 Å from the P1 or R5P binding site [163]. The effect on I_{320} formation of *Pf*Pdx1 could therefore suggest that some long range interactions could be involved from the P3 site that promote R5P binding and initial substrate modulation.

Surprisingly, the RHE triple mutant did not form I_{320}, and sheds new light on the importance of these residues in *Pf*Pdx1. The RHE residues, located on the loop between β3 and α3, was previously shown to confer dodecamer assembly, and subsequently dictated *Pf*Pdx2 binding and activation [133]. Lack of I_{320} formation in the RHE mutant indicates that these residues are intricately involved in R5P binding, additionally taking part in active site reorganisation during dodecamer assembly. Indeed a glycine residue (G84) located on the same loop region as the RHE residues was shown to have H-bonded contacts with D110 which forms part of the G3P P3 binding site in *Sc*Pdx1 [163]. These RHE residues in *Pf*Pdx1 may therefore participate in long-range interactions, communicated through the G3P binding site, which results in the formation of I_{320}.

3.5. Conclusions

Compounds were identified that could inhibit *Pf*Pdx1. These compounds were structurally similar to R5P and had reactive C1 groups, such as aldehyde and hydrazide groups. The MOA was proposed to involve binding in the R5P-binding site of *Pf*Pdx1. The most potent inhibitor of *Pf*Pdx1 attenuated the proliferation of *in vitro* cultured *P. falciparum* parasites, and was suggested to target PLP biosynthesis. Transcriptomics and proteomics were used to further verify whether the compound affected *Pf*Pdx1 and PLP-related processes and is discussed in Chapter 4.